Parametric Microwave Amplification using a Tunable Superconducting Resonator

by

Chung Wai Sandbo Chang

A thesis
presented to the University of Waterloo
in fulfilment of the
thesis requirement for the degree of
Master of Applied Science
in
Electrical and Computer Engineering

Waterloo, Ontario, Canada, 2015

Author’s Declaration

I hereby declare that I am the sole author of this thesis. This is a true copy of the thesis, including any required final revisions, as accepted by my examiners.

I understand that my thesis may be made electronically available to the public.

Chung Wai Sandbo Chang

Abstract

In this Master thesis, I present a theoretical description and experimental measurements of a tunable microwave resonator operated as a parametric amplifier. Superconducting parametric amplifiers have attracted great interest in recent years as it has been demonstrated that they can operate with a noise performance at the standard quantum limit.

Parametric amplification is achieved in the devices by modulating the electrical length of the resonator at twice the resonance frequency. The device measured in this thesis consists of a quarter-wavelength microwave resonator fabricated in a thin-film aluminum coplanar waveguide geometry. With a termination to ground through a Superconducting Quantum Interference Device (SQUID), the boundary condition of the resonator becomes sensitive to an applied magnetic field. This enables the tuning of the resonance frequencies, using a DC magnetic field, over a wide frequency range of 670MHz. Similarly, an AC magnetic field then allows for the modulation of the resonator electrical length at microwave frequencies.

We characterized the device by first measuring the DC tuning curves of the 2nd and 3rd harmonics of the resonator, around 4 GHz and 6 GHz respectively. We then studied parametric amplification in the device when the electrical length was modulated at approximately twice the resonance frequency of one of the modes. We scanned the pump frequency and pump power over a wide range to study the region in parameters which gives parametric gain. We performed an in-depth parameter sweep over this region, identifying pump parameters that provided maximum gain and maximum system noise improvements compared the following HEMT amplifier.

We find that the use of the parametric amplifier can improve the system noise temperature by more than 10 dB compared to a start-of-the-art commercial HEMT amplifier. This implies a performance near the standard quantum limit.

Acknowledgements

With possibilities bounded only by imagination, and the connection to a wide range of knowledge, it's an amazing research field I have been brought into. For all the opportunities and the patience I have been given, I want to thank my supervisor Christopher Wilson. Within my two years in the group, I was given chances travelling to visit other universities and attend summer schools, which further opened me to this wild world of science. Chris has been guiding me not only with studying the knowledge I am fascinated by, but more importantly a construction of sense about being an engineer and a scientist, with his insightful way of thinking he can always understand the root of problems and give valuable advices.

Secondly I want to thank Pol Forn-Diaz, our postdoctoral fellow in the group. During the time when Chris was unavailable Pol was the only mentor we could rely on. I learnt a lot from his professional attitudes towards every details, both in theory and practical work. A large portion of my knowledge about low temperature physics came from the inspiring discussions with Pol, and the chances of seeing the right ways things should be done.

I want to attribute the thesis to Michaël Simoen, without his generous sharing of the parametric amplifier samples this thesis would not have been possible. Michaël is experienced in the similar experiments and has taught me much about the use of equipment and various measurement techniques. Though short, it was a great time working with and learning from him when he was in Waterloo helping Chris to build the laboratory.

I am grateful to have all the helps from other group members and colleagues in IQC. Vadiraj A.M., joining as a senior student, has given me guidance over his skills in nanofabrication in the cleanroom, as well as the hands-on work in daily lab operations. My thanks also go to many others summer students, despite of only a few months working together, I enjoyed every single discussion with them. Often hearing from them about their current studies was inspiring to me.

Finally, I am thankful to my mother and grandma. Letting me go and pursue my dream was not an easy decision, yet as always they put me and my will in advance of anything else. Not for a day I don't remember what I have been given, which then I can remind myself to endure every new challenge.

Contents

List of Figures

1. Introduction

1.1. Motivation

Superconducting circuits operating in the microwave frequency domain have been under rapid research for their potential in realizing quantum computation systems and networks with scalability [1] [2] [3] [4] [5]. It requires the use of dilution refrigerators to cool the quantum bit (qubit) implemented as an artificial atom with circuit elements. The circuit is cooled approximately to 10-20 mK (degree milli-Kelvin) in temperature, in order to avoid thermal excitations, and to allow dissipationless signal transfer. The signal is then sent in and out through a chain of microwave transmission lines, where the first low noise amplifier sitting at 4 degree Kelvin (K) stage, microwave source and detectors stay at room temperature.

As qubits operate at a very low microwave intensity, there are difficulties in differentiating between the collected information and the base noise of common microwave digitizers, which therefore required the use of microwave amplifiers along the measurement chain the signal from the qubit to the detectors.

Quantitatively, the qubit transition energy is $\hbar\omega$ at a given working frequency. HEMT amplifiers (High electron mobility transistor) are widely used at the intermediate stages of the measurement chain as the first stage of signal amplification. Having a noise temperature as low as $T_N = 2K$, this still corresponds to $7\hbar\omega$ for operating at 6 GHz.

In terms of noise propagation of microwave signal, we would need the first, low-noise amplifier to be as close to the qubit as possible, ideally on the same superconducting circuit of the qubit. The HEMT amplifier is designed to work at a higher temperature due to their heat generation, which makes it sit at a different temperature stage inside the dilution refrigerator. This means that the system noise temperature will be higher because of losses.

1.2. Parametric Amplification

These strict requirements on low-noise amplification have led to interest in quantum limited amplifiers [6]. One such successful implementation is the Josephson parametric amplifier (JPA), which makes use of superconducting tunnel junctions called Josephson junctions, as tunable inductive elements. This allows JPAs to achieve a low-noise amplification operating at the same temperature stage as the qubit without generating heat. This can then improve the signal-to-noise ratio when comparing to implementations without these devices. Parametric amplification requires the modulation of a parameter of the system, typically either the resonance frequency or the damping of the cavity as the resonator [7], and in this thesis we take into account the former.

Current pumping has been the common implementation of resonance frequency modulation [8], in which the pump signal is sent into the resonator to modulate the Josephson junction inductance. It has been extensively studied and utilized by various groups as signal amplifier. Another implementation namely flux pumping is done by using a microwave signal to oscillate the magnetic field near a resonator terminated by a combination of Josephson junctions, which then has an effect of modulating its boundary condition. When this oscillation is close to twice the resonance frequency parametric amplification is achieved. The flux pumping regime has also been explored both theoretically and experimentally [7] [9].

1.3. Overview

This thesis is written in an effort to provide a self-contained description of a flux-pumped variant of the JPA, with a quarter-wavelength microwave resonator implemented using thin-film aluminum deposited on silicon as a coplanar waveguide, operating in at the temperature when the aluminum is superconducting.

We start by discussing the basic superconducting elements covering the Josephson junctions and SQUID. Then we will move on to microwave theory, mainly focusing on transmission line, waveguide resonator and resonator coupling to transmission line. After that we will go through a brief discussion on the parametric process and amplification.

We will then move forward to the implementation, outlining the method of control and measurement of the JPA. We will see tuning of resonance frequency, the effect on resonance frequency by pumping and strong signal power. Finally we will analyse the behaviour of the device, understanding the configurations which gives maximum gain and improvement in signal-to-noise ratio brought by the JPA.

2. Theory

2.1. Superconductivity

In a similar sense as water freezes, condensing from its liquid phase to solid phase upon cooling down below zero degree Celsius and under a certain air pressure, a number of metallic elements will undergo a change from their normal phase to superconducting phase when some conditions are met. The two main criteria are the material's critical temperature and critical field. When this is satisfied by being below the both, most metals will become superconducting. Characterized by their loss of resistivity, they can pass DC current with zero dissipation, and high frequency signal with very little loss in signal power. This allows us to build a resonator with low internal loss, where the generated photons can build up in the cavity, and thus be effectively transferred to the transmission line.

The root of superconductivity in metals can be understood as an effective attraction between the electrons mediated by phonons. Phonons are the quantized description of lattice vibrations. This attraction leads to the formation of electron pairs called Cooper-pairs, described by the BCS theory. [10] The Cooper-pairs condense into a macroscopic quantum state. The macroscopic wave function of the Cooper-pairs can be written as [9]:

$$\psi(\boldsymbol{r}) = \sqrt{\rho(\boldsymbol{r})}\boldsymbol{e}^{\boldsymbol{i}\theta(\boldsymbol{r})}$$

where $\rho(\boldsymbol{r})$ is the pair density, and $\theta(\boldsymbol{r})$ is the quantum mechanical phase. Roughly speaking, the absolute square of the wave function, $|\psi(\boldsymbol{r})|^2 = \psi^*\psi$, tells us the density of the Cooper-pairs at a given position.

2.1.1. Josephson Junction

The complex magnitude of the above wave function can be seen as a constant over a block of superconducting material. When the superconducting material is contacting an insulating material, the wave function leaks into the insulating block, with its complex magnitude $|\psi(r)|$ decaying exponentially with distance. Now if we have two superconducting blocks sandwiching a thin, insulating barrier, for instances, two thin-film aluminum (100nm) separated by an aluminum oxide layer of 1nm thick, then the two wave functions of the two superconducting film will be able to extend into the oxide layer, forming a superconducting junction known as Josephson junction [11]. In this case, the two superconductors form a weak link that allows supercurrent to flow through the oxide layer. Josephson described the junctions with two governing equations:

1. Current-phase relationship (DC Josephson effect)

$$I = I_c \sin(\phi)$$

where ϕ is the phase change of the Cooper-pair wave function across the junction. I_c is the critical current of the junction, describing the maximum supercurrent that can flow through the junction before the junction starts to become resistive.

From the normal state resistance R_n of a junction formed by superconducting materials, and the corresponding superconducting gap Δ of that material which tells us the energy of photons needed to break Cooper-pairs, we can approximate its critical current using the Ambegaokar-Baratoff formula:

$$I_c = \frac{\pi\Delta}{2eR_n}$$

The DC Josephson equation connects the current flowing through the junction to the phase difference of the Cooper-pairs wave function across the junction. Its importance will be more obvious when we combine it with the 2nd governing equation of Josephson junction.

2. Phase evolution equation (AC Josephson effect)

$$V = \frac{\hbar}{2e}\frac{d\phi}{dt} = \frac{\Phi_0}{2\pi}\frac{d\phi}{dt}$$

where e is the charge of the electron, 2e therefore denotes the charge of one Cooper-pair.

The equivalent expression on the right utilizes the concept of magnetic flux quantization, with the term flux quantum, $\Phi_0 = h/2e$, as a constant acting as the base unit of magnetic flux threading through a superconducting loop.

This equation evidently connect the voltage across a Josephson junction, to the rate of change in phase difference across it. If we take the time derivative of the Josephson current-phase relationship, we can then substitute it back to the Gor'kov phase evolution equation to get the following:

$$\frac{dI}{dt} = I_c \cos(\phi)\frac{d\phi}{dt}$$

$$V = \frac{\Phi_0}{2\pi}\frac{d\phi}{dt} = \left[\frac{\Phi_0}{2\pi}\frac{1}{I_c\cos(\phi)}\right]\frac{dI}{dt}$$

If we then compare the above to the equation describing the voltage drop across an arbitrary inductor:

$$V = L\frac{dI}{dt}$$

We can observe that the Josephson junction behaves like an inductor, with the inductance depending nonlinearly on the phase difference across the junction due to tunneling $L = \frac{\Phi_0}{2\pi}\frac{1}{I_c\cos(\phi)}$. In order for this inductance to be controllable, we can connect two Josephson junctions in parallel, forming a superconducting loop called a Superconducting Quantum Interference Device (SQUID). Before further proceeding to the description of the SQUID as a tunable inductor, we will first review the connection between the Cooper-pair wave function and the magnetic field threading through a superconducting loop.

2.1.2 Superconducting loop

Consider a charged object moving along a closed loop L in the presence of magnetic field, the canonical momentum will be

$$\boldsymbol{p} = m\boldsymbol{v} + q\boldsymbol{A}$$

where m, **v**, and q are the corresponding mass, velocity operator, and charge respectively; **A** is the vector potential operator corresponding to the magnetic field $\boldsymbol{B}$, threading through the closed loop, as $\boldsymbol{B} = \nabla \times \boldsymbol{A}$.

The quantum mechanical operator for momentum can be expressed as $-i\hbar\nabla$. Considering only the components along the loop, assuming constant Cooper-pair number density, we can obtain

$$-i\hbar\nabla\psi(\boldsymbol{r}) = (m\boldsymbol{v} + q\boldsymbol{A})\psi(\boldsymbol{r})$$
$$\hbar\nabla\theta(\boldsymbol{r}) = m\boldsymbol{v} + q\boldsymbol{A}$$

Integrating along the closed loop:

$$\hbar \oint_L \nabla\theta_l dl = m \oint_L v_l dl + q \oint_L A_l dl$$

$$\hbar \Delta\theta_l = m \oint_L v_l dl + q \int (\nabla \times \boldsymbol{A}) \cdot d\boldsymbol{S}$$

$$= m \oint_L v_l dl + q \int \mathbf{B} \cdot d\boldsymbol{S}$$

$$\frac{\hbar}{q} \Delta\theta_l = \frac{m}{q} \oint_L v_l dl + \Phi_{applied}$$

Recognizing that current density $\boldsymbol{J} = n_s q \boldsymbol{v}$,

$$\frac{\hbar}{q} \Delta\theta_l = \frac{m}{n_s q^2} \oint_L J dl + \Phi_{applied}$$

In order for the Cooper-pair wave function to be single valued, the line integral over the phase θ around a closed loop has to be an integer multiple of 2π [12], such that:

$$\frac{\hbar}{q} 2\pi \mathrm{n} = \frac{m}{n_s q^2} \oint_L J dl + \Phi_{applied}$$

Recalling q for Cooper-pair is $2e$, we arrive at:

$$\Phi_0 \mathrm{n} = \frac{m}{n_s (2e)^2} \oint_L J dl + \Phi_{applied}$$

This is the fluxoid quantization of all superconducting loops.

We can consider a loop deep within a superconductor, such that J is zero or negligible without applied current [12], then we have the connection between the phase change of the Cooper-pair wave function connected to vector potential as

$$\oint_L \nabla\theta_l dl = \frac{q}{\hbar} \oint_L A_l dl$$

2.1.3 SQUID

Similar to a superconducting loop, in a SQUID loop, the phase change also integrates to an integer multiple of 2π, i.e. $\oint_L \nabla\theta_l dl = 2\pi n$. However, in addition to a closed-loop integral of the vector potential, the phase change across the two junctions due to tunneling will also contribute to the total phase change (which is always $2\pi n$). Qualitatively, it can be understood as a balance between the phase change by the flux and that by tunnelling through junctions, where they have to sum up to $2\pi n$. Consider the following SQUID loop:

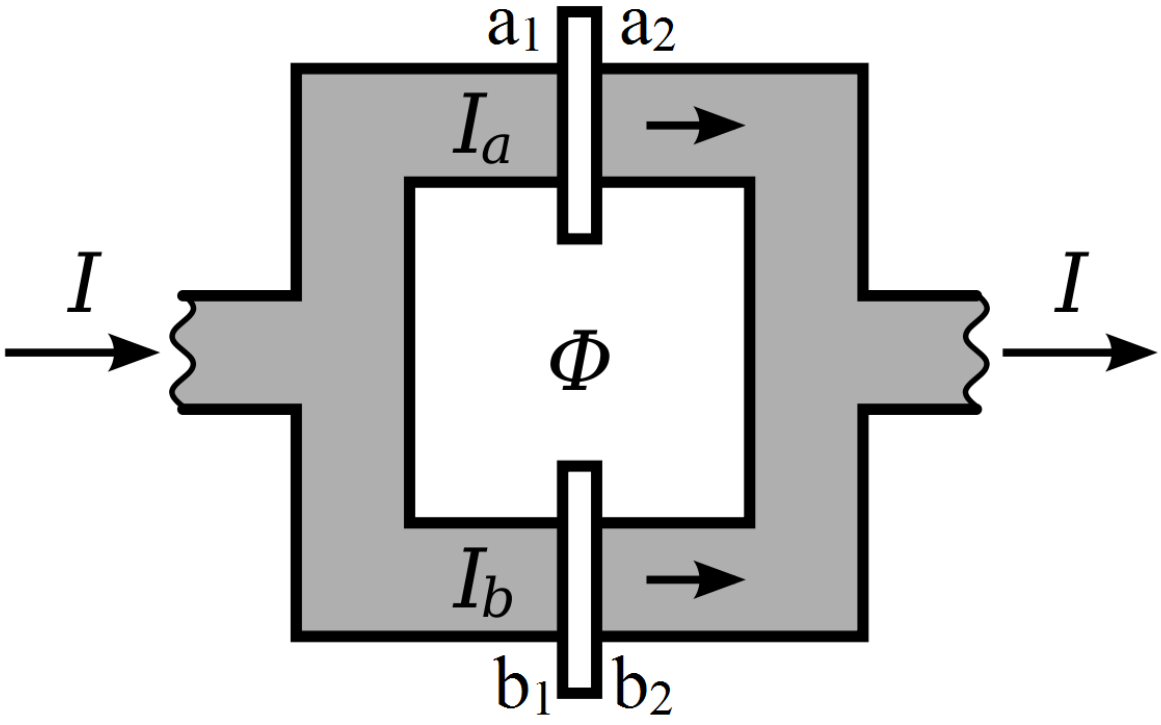

Figure 1. A SQUID loop. A parallel connection of two Josephson junctions. It is often characterised by the area enclosed by the loop, together with the junctions dimension. Adopted freely from wikipedia: https://en.wikipedia.org/wiki/SQUID

By integrating along the loop in 4 subsections, clock-wise along the center of the above SQUID loop in Figure 1, $(a_2\ to\ b_2)$, $(b_2\ to\ b_1)$, $(b_1\ to\ a_1)$, and finally $(a_1\ to\ a_2)$, using the integral relation between vector potential and phase change of Cooper-pairs we have:

$$\oint_L \nabla\theta_l dl = \left(\frac{q}{\hbar}\int_{a_2}^{b_2} A_l dl\right) + \left(\frac{q}{\hbar}\int_{b_2}^{b_1} A_l dl + \phi_a\right) + \left(\frac{q}{\hbar}\int_{b_1}^{a_1} A_l dl\right) + \left(\frac{q}{\hbar}\int_{a_1}^{a_2} A_l dl + \phi_b\right) = 2\pi n$$

where ϕ_a and ϕ_b are the phase change of Cooper-pairs due to tunnelling through the junction. Rearranging, we get

$$\phi_a + \phi_b + \frac{q}{\hbar}\oint_L A_l dl = 2\pi n$$

Then by using stroke theorem we will have (2.1.3a)

$$\phi_a + \phi_b + 2\pi\frac{\Phi_{applied}}{\phi_0} = 2\pi n$$

Now we have seen the way to modulate the phase across the junction by means of an externally applied flux, we can calculate the SQUID inductance accordingly to the modulation.

In most cases and in this thesis, we consider a SQUID loop with identical junctions, a and b, on both sides such that the critical current I_c of the junctions are the same. Consider a current passing through the SQUID as:

$$I = I_a + I_b = I_c \sin(\phi_a) + I_c \sin(-\phi_b)$$

$$I = 2I_c \cos\left(\frac{\phi_a + \phi_b}{2}\right) \sin\left(\frac{\phi_a - \phi_b}{2}\right)$$

$$= I_0 \cos\left(\pi \frac{\Phi_{applied}}{\Phi_0}\right) \sin(\phi_{dc})$$

where we define $\phi_{dc} = \frac{\phi_a - \phi_b}{2}$ as the effective phase difference across the SQUID, and $I_0 = 2I_c$ is the effective critical current. The negative sign of ϕ_b comes from the fact that we were integrating in a direction opposite to the assumed DC current direction in the above loop integral at junction b. (Current passing through the SQUID from left to right on both junctions. Loop integral is towards right at junction a, but towards left at junction b).

This is essentially the Josephson current-phase relationship, but instead for a single junction it now describes that of a SQUID. In the same manner for a junction, we can now treat a SQUID as a single junction, with effective phase drop as the defined ϕ_{dc}. Then we can approximate $\sin(\phi_{dc})$ about a small static phase drop ϕ_0 to first order, followed by doing the time derivative of I. Substituting the result back to the phase evolution equation we can obtain the equivalent inductance of the SQUID.

With the assumption of no pumping such that $\Phi_{applied}$ is time independent, the SQUID inductance is [9]:

$$L_s = \frac{\Phi_0}{2\pi} \frac{1}{I_0 \left|\cos\left(\pi \frac{\Phi_{applied}}{\Phi_0}\right)\right| \cos(\phi_0)}$$

and by further assuming a low signal power, thus ϕ_0 is small, we have:

$$L_s = \frac{\Phi_0}{2\pi} \frac{1}{I_0 \left|\cos\left(\pi \frac{\Phi_{applied}}{\Phi_0}\right)\right|} = \frac{L_{s0}}{\left|\cos\left(\pi \frac{\Phi_{applied}}{\Phi_0}\right)\right|}$$

where $L_{s0} = \frac{\Phi_0}{2\pi} \frac{1}{I_0}$ is the unbiased SQUID inductance when the applied flux threading through the SQUID is exactly an integer multiple of Φ_0, defined in a similar way as for a Josephson junction. The unbiased SQUID inductance based on a Josephson junction of known room temperature resistance is $L_{s_0} = \frac{\Phi_0 e R_n}{\pi^2 \Delta}$.

2.2. Microwave Theory

In the implementation of superconducting circuit, it is often favourable to work in the microwave regime where the frequency of signal ranges from 1 GHz to 16 GHz, such that the influence of thermal noise and $1/f$ noise is reduced, while commercially available microwave sources and detectors can be adopted. However this also transforms the analysis of the system from the view point of circuit theory to transmission line theory, where the latter becomes important when the wavelength is comparable to the longest structures of the superconducting circuit components.

2.2.1. Transmission Line

Microwave signal propagates on a superconducting circuit in a similar way as they propagate along a coaxial cable. The current flows along the surface of the inner and outer conductor of the waveguide. This can be visualized by considering a longitudinal wave of electrons, where the compressions and rare fractions are propagating in an opposite direction along the center line and ground plane, forming propagating voltage differences between the two conductors, as described by the following picture:

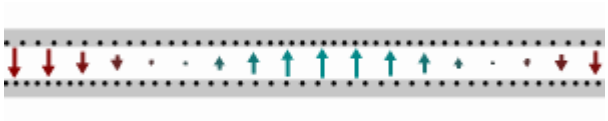

Figure 2. A waveguide model. Propagating microwave signal along a waveguide, with the dots on two sides being electrons on ground and center line. The arrows indicate the voltage profile between the two conductors along the axial direction. Then they move along the waveguide as if a wave is propagating along a string. Adopted freely from Wikipedia: https://en.wikipedia.org/wiki/Telegrapher's_equations

The current and voltage at any point along the waveguide can therefore be described by the telegrapher's equations, similarly to those of wave propagation towards both directions. With reference to an origin position $z = 0$ at the input port of the waveguide on the left, it can be expressed as [13]:

$$V(z) = V_0^+ e^{-\gamma z} + V_0^- e^{\gamma z}$$
$$I(z) = I_0^+ e^{-\gamma z} - I_0^- e^{\gamma z}$$

where the term $\gamma = \alpha + j\beta$ is the propagation constant decided by the physical properties of the waveguide. α is the attenuation, and β is the phase change per unit length of the propagation. $V^{\pm}$ *and* $I^{\pm}$ refers to the amplitude of the voltage and current for the wave travelling towards the right (+) and left (-). The impedance at a given position is then defined as $Z(z) = V(z)/I(z)$.

For a superconducting circuit we may assume a lossless line and reduce the propagation constant to $\gamma = j\beta = j\omega\sqrt{L_0 C_0}$, with L_0 and C_0 the inductance and capacitance at any point along the axial direction of the waveguide. We can find the characteristic impedance as $Z = \sqrt{L_0/C_0}$ that connects the voltage and current at that point along the transmission line.

In the thesis the amplifier is implemented on coplanar waveguide (CPW) made from thin-film aluminum. The basic structure is a narrow metallic center line surrounded by two semi-infinite ground planes separated by equal distance, all sitting in the same plane on top of the substrate, where the propagation property is determined by the geometry, as illustrated below:

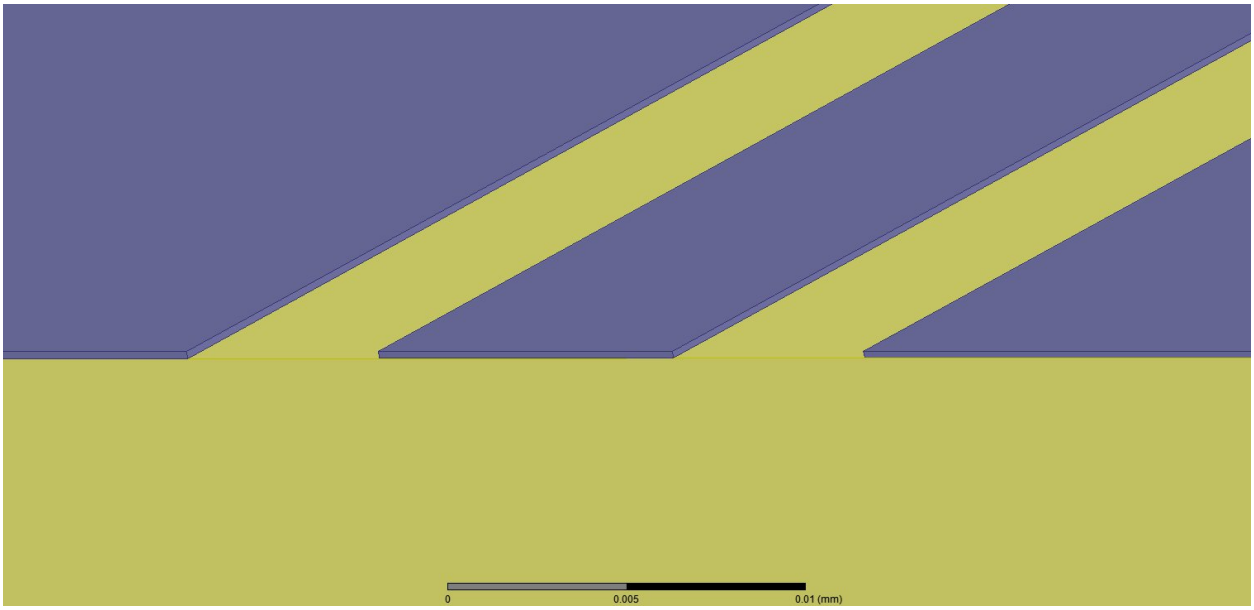

Figure 3. Example of coplanar waveguide. A CPW waveguide drawn in HFSS (High Frequency Structure Simulator) as the implementation of the transmission line, where the blue traces are metal on the yellow substrate.

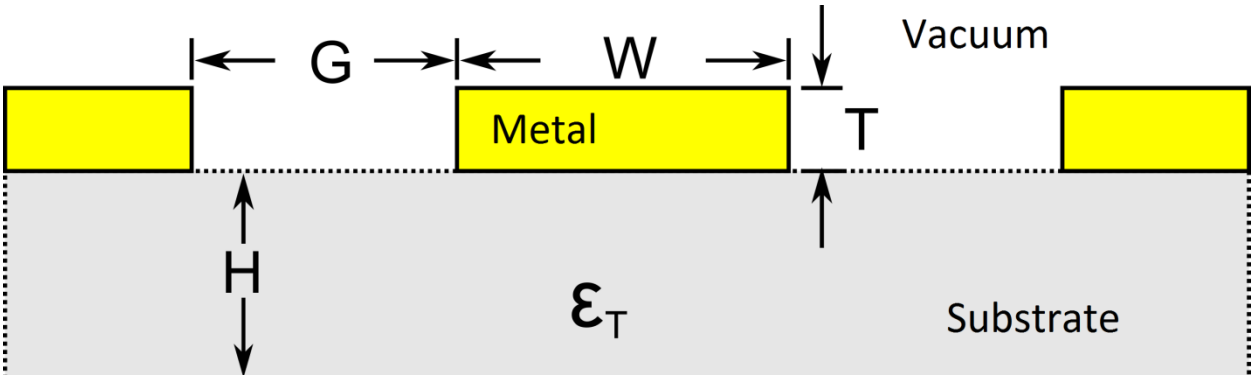

Figure 4, A cross section of a CPW waveguide. The characteristic impedance is determined by the inductance of the center line, and the capacitance it forms with the ground plane. They then depend on the geometry as the separation between the ground and the centerline (G),the width of the centerline (W), and the substrate we use which has the dielectric constant (ϵ_T). Usually for superconductor, by keeping the G to W ratio to be around 6.5 we can get the characteristic impedance of the transmission line as 50Ohm. Adopted from Wikipedia: en.wikipedia.org/wiki/Coplanar_waveguide#/media/File:Cross_Section_of_Coplanar_Waveguide_Transmission_Line.png

2.2.2. Resonator

The implementation of the resonator for the parametric amplifier was done by introducing a coupling capacitor on one end of the transmission line, and have it terminated by a SQUID as a tunable inductor to ground on the opposite end, forming a quarter-wavelength resonator, which creates a cavity where it can only be voltage anti-node at the capacitor, and voltage node at the SQUID, such that only waves with their odd multiple of quarter-wavelength equivalent to the cavity's electrical length are allowed in the cavity. We will first work on a bare resonator design, ignoring the effect of the SQUID.

For a bare resonator terminated with ground, where the incident wave is reflected by the termination with a phase shift of π, then we have $V_0^- = -V_0^+$ and $I_0^- = -I_0^+$, and $Z(z)$ becomes

$$Z(z) = jZ_0 \tan(\beta l)$$

From the analysis of transmission line resonator, we can approximate its fundamental mode as the resonance of a lumped element resonator where the elements R, L and C are connected in parallel. [9] [13], with the frequency noted as $f_0 = \frac{c}{4l\sqrt{\epsilon_{eff}}}$, where c is the the speed of light, l is the cavity's physical length and ϵ_{eff} is the effective dielectric constant, being roughly the average of the dielectric constants of air and the substrate in CPW implementation. For higher order modes of a quarter-wavelength resonator, the resonance frequencies can be approximated as, for m^{th} mode, $f_m = (2m+1)f_0$. This also applies to the modified quarter-wavelength resonator discussed in the later sections. On knowing how to design the waveguide resonator for the concerning frequency, the next important step will be to design the coupling between the transmission line and the resonator.

2.2.3. Coupling

The coupling of a resonator to another medium is usually characterized by their Q-factors. The internal Q-factor, Q_0, refers to the rate of photon lost inside the cavity due to dissipation. It is defined as $Q_{0_{series}} = 1/\omega_0 RC$ and $Q_{0_{parallel}} = \omega_0 RC$ for series and parallel resonator respectively. We always want the internal Q-factor to be as high as possible in order that the generated photons are not destroyed within the cavity. The external Q-factor, Q_e, refers to the rate of photon leaving the cavity for the coupled medium, and we have the loaded or measured Q-factor $Q_m = (Q_0^{-1} + Q_e^{-1})^{-1}$ as the measurable Q-factor. Thus, we have the coupling coefficient defined as $g = \frac{Q_0}{Q_e}$, which determines which coupling case it will be.

They can be divided into 3 types:

$g < 1$, under-coupling

$g = 1$, critical-coupling

$g > 1$, over-coupling.

The first two types of coupling will not allow the photons to leave the cavity efficiently to be detected. For the parametric amplifier, we require over-coupling in order for the generated photons inside the cavity to leak to the transmission line and be measured. In order to know the needed coupling capacitance, the following two methods can be used.

1. Estimation from bare resonator frequency

The coupling the resonator to the transmission line is done by using a capacitor C_c, which can be understood as connecting a series capacitor to the resonator [13], we can write:

$$z = \frac{Z}{Z_0} = \frac{j\left(Z_0 tan\beta l - \frac{1}{\omega C}\right)}{Z_0} = j\left(tan\beta l - \frac{1}{b_c}\right)$$

where $b_c = Z_0 \omega C_c$ is defined as normalized susceptance of the coupling capacitor C_c.

At resonance we will have $z = 0$, which translates to $tan\beta l = \frac{1}{b_c}$. In practice $b_c \ll 1$ as the capacitors are usually in tens of femto farads, and $\omega_0 = 2\pi \times 1GHz$, we will assume $\beta l = \pi/2$. The exact result can instead be found by solving the transcendental equation $tan\beta l = \frac{1}{b_c}$.

By expanding z in Taylor series about the first resonant frequency ω_1 to first order, and with the above conditions, we have

$$z(\omega) \approx \frac{j\pi(\omega - \omega_1)}{2\omega_1 b_c^2}$$

From the above lossless normalized impedance, the effect due to loss can be modelled by using the perturbation method, with replacing ω_1 with $\omega_1\left(1 + \frac{j}{2Q_0}\right)$ [13], we find the lossy normalized impedance as:

$$z(\omega) \approx \frac{\pi}{4Q_0 b_c^2} + j\frac{\pi(\omega - \omega_1)}{2\omega_1 b_c^2}$$

which is, by comparing to the forms of lumped element resonator, a series RLC resonator response. We can re-write $g = Q_0/Q_e = Z_0/Z_{in}$ at resonance.

For a superconducting resonator, the internal Q-factor is usually very high (>100 thousands), thus we can focus on finding the photon leak towards transmission line, which is controlled by Q_e. From g,

$$g = \frac{Q_0}{Q_e} = \frac{Z_0}{Z_{in}}$$

$$Q_e = \frac{\pi}{4b_c^2}$$

and as long as Q_e is much lower than the internal Q-factor, the resonator will be strongly over-coupled. This is done by choosing the capacitance value which corresponds to b_c.

The above, however, is a perturbative method and was approximated at a resonance frequency without taking into account the effect of the coupling capacitor. It allows an estimation of the coupling capacitance needed given the required Q_e, or vice versa. Depending on the type of coupling we need, the perturbative method may suffice if we simply require the resonator to be strongly over coupled.

2. Transformation of the coupling circuit by Norton equivalent

A method outlined in [9] and [14] takes into account the per unit length inductance and capacitance of the resonator. This allows us to calculate the resonant frequency shift due to the coupling.

Consider a series RC network with the coupling capacitor C_c, and the transmission line with characteristic impedance Z_0, we can re-arrange them into a parallel RC network, then we can calculate the corresponding R' and C' of that parallel RC network in terms of the series R and C.

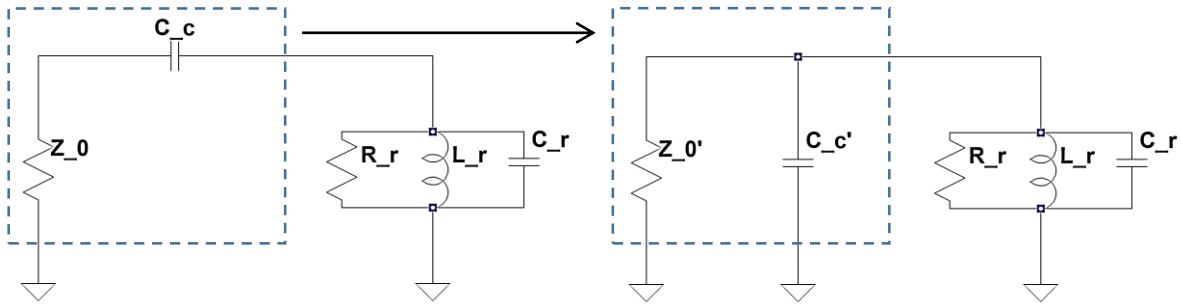

Figure 5. The transformation from series RC circuit to parallel RC circuit. Left: original circuit, with transmission line of characteristic impedance Z_0 and coupling capacitor C_c connected in series with the parallel RLC circuit modelling the quarter-wavelength resonator Right: Transformed circuit by finding the Norton equivalent Z_0 and C_c, which are connected instead in parallel to the resonator

In Figure 5, by setting the impedance of the left and right boxed sections equivalent, we have:

$$Z_0 - \frac{i}{\omega C_c} = \frac{Z_0' \left(-\frac{i}{\omega C_c'}\right)}{Z_0' - \frac{i}{\omega C_c'}}$$

$$Z_0 - \frac{i}{\omega C_c} = \frac{Z_0'}{1 + \omega^2 {C_c}'^2 {Z_0'}^2} - \frac{i\omega {C_c}' {Z_0'}^2}{1 + \omega^2 {C_c}'^2 {Z_0'}^2}$$

with which we can separate them into the real part and imaginary part. Q_0 and ω_0 should remain unchanged throughout the transformation, therefore we apply $\omega R'C' = Q_{0_{parallel}} = Q_{0_{series}} = \frac{1}{\omega RC}$, and get:

$$Z_0' = Z_0 \frac{1 + \omega^2 C_c^2 {Z_0}^2}{\omega^2 C_c^2 {Z_0}^2} \approx \frac{Z_0}{\omega^2 C_c^2 {Z_0}^2}$$

$${C_c}' = C_c \frac{1}{1 + \omega^2 {Z_0}^2 C_c^2} \approx C_c$$

under the assumption that $\omega Z_0 C_c \ll 1$.

Then, with $R_r = \infty$ for a low loss resonator, the parallel Z_0' and C_c' combine with the $\lambda/4$ parallel resonator, forming a new resonator with different resonant frequency.

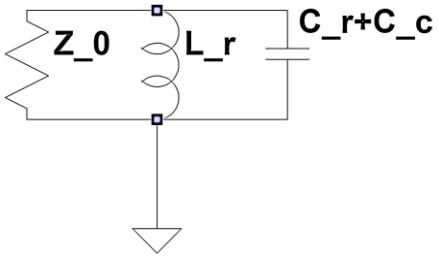

Figure 6. Resonator formed with the transformed parallel RC. It results in a parallel ZLC resonator

With coupling capacitor C_c:

$$\omega_{0_{coupled}} = \frac{1}{\sqrt{L(C + C_c)}}$$

The newly formed parallel resonator takes into account the loss to the line due to coupling through C_c, such that we have its internal Q-factor of the transformed circuit, as the external Q-factor of the original circuit:

$$Q_{loaded_{original}} \approx Q_{e_{original}} = Q_{0_{transformed}} = \frac{C_r + C_c}{\omega_{0_{coupled}} C_c^2 Z_0}$$

Then by substituting C with $(C_R l)/2$, where C_R is the resonator's per unit length capacitance to ground, and L with L_R, the resonator total inductance, one would be able to calculate the external Q-factor and the coupling capacitance needed. Once the Q-factor for the fundamental mode is found, the higher order modes Q-factor can be approximated by scaling up the $\omega_{0_{coupled}}$ accordingly. In particular for a quarter-wavelength resonator, $Q_m \approx Q_0/(2m + 1)$.

2.3. Tunable Cavity and Parametric Process

We can now proceed to understanding the parametric process in a SQUID terminated resonator described in [7]. The cavity is made tunable by the introduction of a SQUID as a parametric inductance, sitting as an interface between the quarter-wavelength transmission line section and the ground, to form a similar resonator as the short circuited quarter-wavelength resonator described in 0. The SQUID acts as a tunable boundary condition for the resonator, which is then controlled externally by the applied magnetic field.

2.3.1. Parallel LC Resonator Model

From the previous section, we have seen that we can approximate a $\lambda/4$ resonator terminated by a short to ground using a parallel RLC resonator model followed by transformation. We can now define the elements as C_c as the coupling capacitance, and L_k, C_k as the resonator inductance and capacitance. R is again assumed to be infinite with a superconducting resonator having negligible loss. Consider the circuit below:

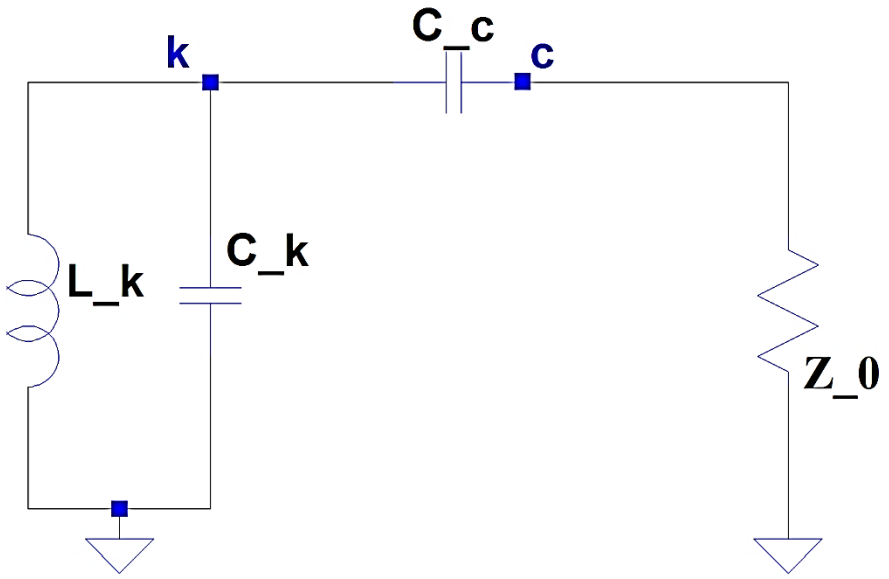

Based on the expression of microwave as voltage along the transmission line, we will follow the context of quantum network theory described in [15] and then the procedure in [7]. We view the resonator as scattering the incoming field propagating in the transmission line. We use the canonical flux as $\Phi_i(x,t) = \int_{-\infty}^{t} V_i(x,t')dt'$ to denote the flux at each node, where V_i is the voltage at each circuit node with reference to ground. x refers to the position along the transmission line. We take the resonator to be $x = 0$ (node c), and the direction away from the resonator as positive.

Then we have the $\Phi c(x,t) = \Phi_{in}\left(\frac{x}{v} + t\right) + \Phi_{out}\left(-\frac{x}{v} + t\right)$ expressing the total field along the transmission line as the sum of the incoming and outgoing field. We also note that the characteristic impedance of the line is $Z_0 = \sqrt{L_0/C_0}$, and $v = 1/\sqrt{L_0 C_0}$, with v being the speed of the microwave in the line, and L_0, C_0 being the per unit length inductance and capacitance of the line.

By doing the space and time differentiation on $\Phi_c(x,t)$, we can get the boundary condition at $x = 0$ as:

$$-\frac{1}{L_0}\frac{\partial \Phi_c}{\partial x}\Big|_{x=0} = \frac{1}{Z_0}\left(\frac{\partial \Phi_c}{\partial t} - 2\frac{\partial \Phi_{in}}{\partial t}\right)\Big|_{x=0}$$

which connects the input field to that at the resonator. It follows that the current through the capacitive and inductive elements through the circuit can be related to flux with the following equations:

$$I_L = \frac{\Delta\Phi}{L}$$

$$I_C = C\frac{d^2(\Delta\Phi)}{dt^2}$$

where $\Delta\Phi$ is the difference of the node flux across that element. From the boundary condition, we can find the current at node c,

$$-\frac{1}{L_0}\frac{\partial \Phi_c}{\partial x}\Big|_{x=0} = \frac{1}{Z_0}\left(\frac{d\Phi_c}{dt} - 2\frac{\partial \Phi_{in}}{\partial t}\right)$$
$$\frac{\Delta x}{L}\frac{\partial \Phi_c}{\partial x}\Big|_{x=0} = \frac{\Delta\Phi_c}{L} = -\frac{1}{Z_0}\frac{d\Phi_c}{dt} + \frac{2}{Z_0}\frac{d\Phi_{in}}{dt}$$

and relate that to the capacitor current as (2.3.1a)

$$C_c\left(\frac{d^2\Phi_c}{dt^2} - \frac{d^2\Phi_k}{dt^2}\right) = -\frac{1}{Z_0}\frac{d\Phi_c}{dt} + \frac{2}{Z_0}\frac{d\Phi_{in}}{dt}$$

Also, by considering KCL at node k and re-arranging:

$$\frac{\Phi_{\mathrm{k}}}{L_k} + C_k\frac{d^2\Phi_k}{dt^2} = C_c\left(\frac{d^2\Phi_c}{dt^2} - \frac{d^2\Phi_k}{dt^2}\right)$$
$$\frac{d^2\Phi_k}{dt^2}(C_c + C_k) + \frac{\Phi_{\mathrm{k}}}{L_k} = C_c\frac{d^2\Phi_c}{dt^2}$$

$$\frac{d^2\Phi_k}{dt^2} + \frac{\Phi_{\mathrm{k}}}{L_k(C_c + C_k)} = \frac{C_c}{C_c + C_k}\frac{d^2\Phi_c}{dt^2}$$

Recall in the previous section we defined the resonant frequency $\omega_0 = 1/\sqrt{LC}$.We can therefore find from the above equation $\omega_0 = 1/\sqrt{L_k(C_c + C_k)}$ and the coupling parameter $\kappa = C_c/(C_c + C_k)$ which describes the coupling to the line (not to be confused with coupling coefficient), and rewrite the equation to (2.3.1b):

$$\frac{d^2\Phi_k}{dt^2} + \omega_0^2\Phi_k = \kappa\frac{d^2\Phi_c}{dt^2}$$

2.3.2. Resonance Frequency Tuning

The cavity can have its resonance frequency tuned by applying a DC flux threading through the SQUID loop, to set a static boundary condition on the grounded end of the resonator through the SQUID, according to the SQUID inductance equation defined in 0. By expanding the characteristic equation of the cavity terminated by a tunable inductor, the frequency tuning equation can be found as [16]:

$$\omega_0(\Phi_{applied}) = \frac{\omega_b}{1 + \frac{L_s(\Phi_{applied})}{L_0 l}}$$

with ω_b being the bare short circuited resonator frequency, L_s being the SQUID inductance defined in 2.1.3, and $L_0 l$ is the total inductance of the quarter-wavelength resonator calculated by its per unit length inductance times the length. This allows one mode of the cavity to span a wide frequency range as large as ω_b, which then we can select a bias point in terms of applied DC flux.

To visualize the modulation, consider a quarter-wavelength transmission line resonator where its electrical length is fixed by its design, i.e. substrate material and resonator dimension.

Having a SQUID at the grounding point, it allows the effective electrical length of the resonator to be changed. Instead of always being a voltage node at the ground in the case of a bare resonator, the SQUID inductance raises or lowers the voltage at that node from zero. The further the SQUID is tuned when the threading flux changes from $n\Phi_0$ to $(n \pm 1/2)\Phi_0$ by the applied field, the further away from zero the voltage it will be at the node.

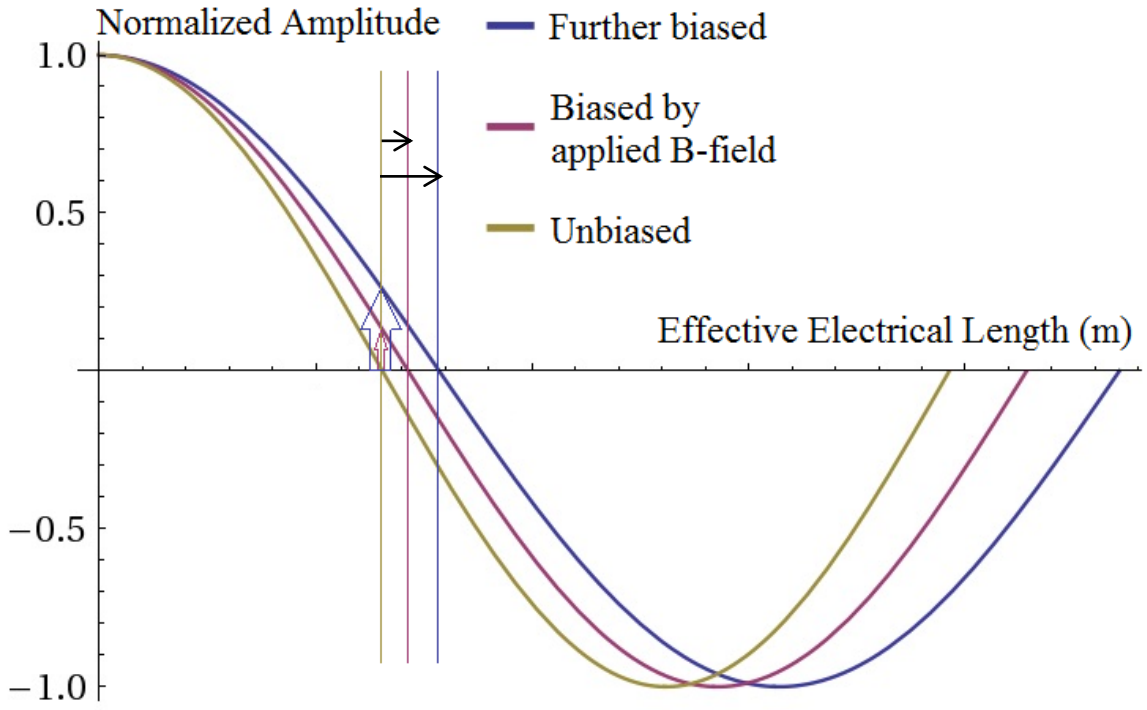

Figure 7. Flux biasing and electrical length modulation of the resonator. (Yellow) Unbiased resonator, (Purple) Resonator biased by externally applied magnetic field (Blue) Further biased resonator by a stronger applied magnetic field. The three vertical lines refers to the positions of voltage nodes of different biasing. Their positions along the x-axis refers to the electrical length of the resonator. When the resonator is biased with a stronger magnetic field, the longer the effective electric length of the resonance will be, thus the biased resonator always have a lowered frequency. In reality the physical length of the resonator is fixed, the extension of the electrical length is achieved by a change in the voltage value at the SQUID, as indicated by the two up arrow.

Then we can see it as having the voltage node sitting further away, effectively the tuned resonator has a longer electrical length than the unbiased resonator, which give rise to a lowered resonance frequency for any tuning. It is also worth noting that the unbiased frequency will be lower than that of a bare quarter-wavelength resonator, from the fact that the SQUID inductance is always nonzero.

2.3.3. Parametric Pumping

On top of the above DC flux bias, we can superimpose a time-varying magnetic flux which is also threading through the SQUID loop, by pumping the circuit with an AC magnetic flux of frequency ω_p and amplitude $\delta\Phi$, which then the applied field takes the form $\Phi_{applied}(t) = \Phi_{dc} + \delta\Phi\cos(\omega_p t)$, and we get the time-dependent frequency [7]:

$$\omega_0^2(t) = \omega_0^2(\Phi_{dc}) + \left.\frac{\partial\omega_0^2}{\partial(\delta\Phi)}\right|_{\delta\Phi=0} \delta\Phi\cos(\omega_p t) = \omega_0^2(\Phi_{dc}) + F\cos(\omega_p t)$$

F is the pump strength which depends on the bias point chosen and the AC flux amplitude, as $F = 2\pi\tan\left(\pi\frac{\Phi_{dc}}{\Phi_0}\right)\frac{\omega_0^3}{\omega_b}\frac{L_s(\Phi_{dc})}{L_0 l}\frac{\delta\Phi}{\Phi_0}$. The modelling of the parametric pumping is based on the modulation of the resonance frequency, the effect of modulation can thus be included by modifying the resonance frequency term defined in (2.3.1b), as (2.3.3a):

$$\frac{d^2\Phi_k}{dt} + \Phi_k\left(\omega_0^2 + F\cos(\omega_p t + \phi)\right) = \kappa\frac{d^2\Phi_c}{dt^2}$$

where ϕ is the phase of the pump with respect to the signal. The signal is assumed to have the form $\Phi_{in}(t) = \Phi_{in}^0\cos\left(\frac{\omega_p t}{2}\right)$, as we will be focusing on degenerate pumping in which the signal frequency will be half of the pump frequency, i.e. $\omega_0 = \omega_p/2$.

As the driving term $F\cos(\omega_p t + \phi)$ is nonlinear, the response cannot be expressed as a linear superposition of functions and thus cannot be solved using Fourier analysis exactly. However the solution can be approximated by using a technique known as harmonic balance [7]. Starting with an ansatz, we express the signal in terms of its in-phase and quadrature components:

$$\begin{aligned}\Phi_i &= q_{i,1}\cos\left(\frac{\omega_p}{2}t\right) - q_{i,2}\sin\left(\frac{\omega_p}{2}t\right)\\ &= \frac{u_i}{2}exp\left(i\frac{\omega_p}{2}t\right) + \frac{u_i^*}{2}\exp(-i\frac{\omega_p}{2}t)\end{aligned}$$

where $i \in \{c,k\}$ refers to the nodes. The coefficients $q_{i,1}$ and $q_{i,2}$ are the amplitude of the in-phase and quadrature components of the signal, which depends on its phase with respect to a reference signal. For convenience it is expressed in the complex representation with $u_i = q_{i,1} + iq_{i,2}$.

Plugging the ansatz into the equations (2.3.3a), we can rearrange and group terms associated with the same frequency ω and get:

$$\begin{aligned}&\left[\left(\omega_0^2 - \left(\frac{\omega_p}{2}\right)^2\right)\frac{u_k}{2} + \frac{F}{2}e^{i\phi}\frac{u_k^*}{2} + \kappa\left(\frac{\omega_p}{2}\right)^2\frac{u_c}{2}\right]exp\left(i\frac{\omega_p}{2}t\right)\\ &+\left[\left(\omega_0^2 - \left(\frac{\omega_p}{2}\right)^2\right)\frac{u_k^*}{2} + \frac{F}{2}e^{-i\phi}\frac{u_k}{2} + \kappa\left(\frac{\omega_p}{2}\right)^2\frac{u_c^*}{2}\right]exp\left(-i\frac{\omega_p}{2}t\right)\\ &+\left[\frac{F}{2}e^{i\phi}\frac{u_k}{2}\exp\left(i\frac{3\omega_p}{2}t\right) + \frac{F}{2}e^{-i\phi}\frac{u_k^*}{2}\exp\left(-i\frac{3\omega_p}{2}t\right)\right] = 0\end{aligned}$$

Each of these collections of terms form a separate algebraic equation, as different harmonics are orthogonal. The coefficients of the sinusoids then form a system of equations. An approximation is done by considering only the lowest harmonic, $\omega_p/2$, ignoring the terms with $3\omega_p/2$, we get the equation

$$\left(\omega_0^2 - \left(\frac{\omega_p}{2}\right)^2\right)u_k + \frac{F}{2}u_k^* e^{i\phi} = -\kappa\left(\frac{\omega_p}{2}\right)^2 u_c.$$

Similarly, we can get from (2.3.1a), again by considering the coefficients of $exp(i\omega_p t/2)$, we have (2.3.3b)

$$-C_c\left(\frac{\omega_p}{2}\right)^2(u_c - u_k) = -\frac{i}{Z_0}\frac{\omega_p}{2}u_c + \frac{i2}{Z_0}\frac{\omega_p}{2}\Phi_{in}^0$$

From the above equation, and by using the boundary condition $\Phi_{out} = \Phi_c - \Phi_{in}$, we can transform it to:

$$u_{out} = \frac{Z_0}{Z_0 + Z_c}u_k + \frac{Z_c - Z_0}{Z_0 + Z_c}\Phi_{in}^0$$

where Z_c is the impedance of the coupling capacitor.

With the limit that $|Z_c|$ at the resonance frequency is much greater than Z_0, we define:

$$\kappa Q = \frac{|Z_C(\omega_0)|}{Z_0} = \frac{1}{Z_0 C_c \omega_0}$$

where $Q = (C_c + C_k)/Z_0 C_c^2 \omega_0$ is the quality factor of the resonator as defined in 2.2.3. Then we can solve for the output in-phase and quadrature components of the signal as:

$$\frac{q_{out,1}}{\Phi_{in}^0} = 1 - 2\frac{1 + \zeta\sin(\phi)}{1 + \Omega^2 - \zeta^2}$$

$$\frac{q_{out,2}}{\Phi_{in}^0} = 2\frac{\zeta\cos(\phi) - \Omega}{1 + \Omega^2 - \zeta^2}$$

with defining the normalized detuning:

$$\Omega = \frac{2Q}{\omega_0}\left(\frac{\omega_p}{2} - \omega_0\right)$$

and normalized drive strength:

$$\zeta = \frac{FQ}{\omega_0\omega_p}$$

In order for the resonator to operate as an amplifier, we will need to have ζ smaller than 1. For $\zeta > 1$, the circuit will be working instead as a parametric oscillator, where the resonator oscillates spontaneously and the solutions above will no longer be applicable. The solutions also suggest a dependence of the quadrature amplitude on the pump phase with respect to the signal; this is a characteristic of parametric amplification which can also be observed in the optical domain [17].

3. Implementation

A parametric amplifier sample fabricated by Michaël Simoen was measured to examine its gain and improvement in signal-to-noise ratio.

In this section we will first describe the design characteristics of the sample. Then we will go through the measurement workflow, describing how we can tune the resonance frequency and pump the circuit. We will measure the gain from parametric amplification, and compare the signal-to-noise ratio between the cases with and without the amplification.

3.1. Resonator circuit design

The microwave circuit was constructed by a deposition of thin-film Aluminum on a Silicon wafer using e-beam lithography. The below shows the CAD drawing of the measured sample:

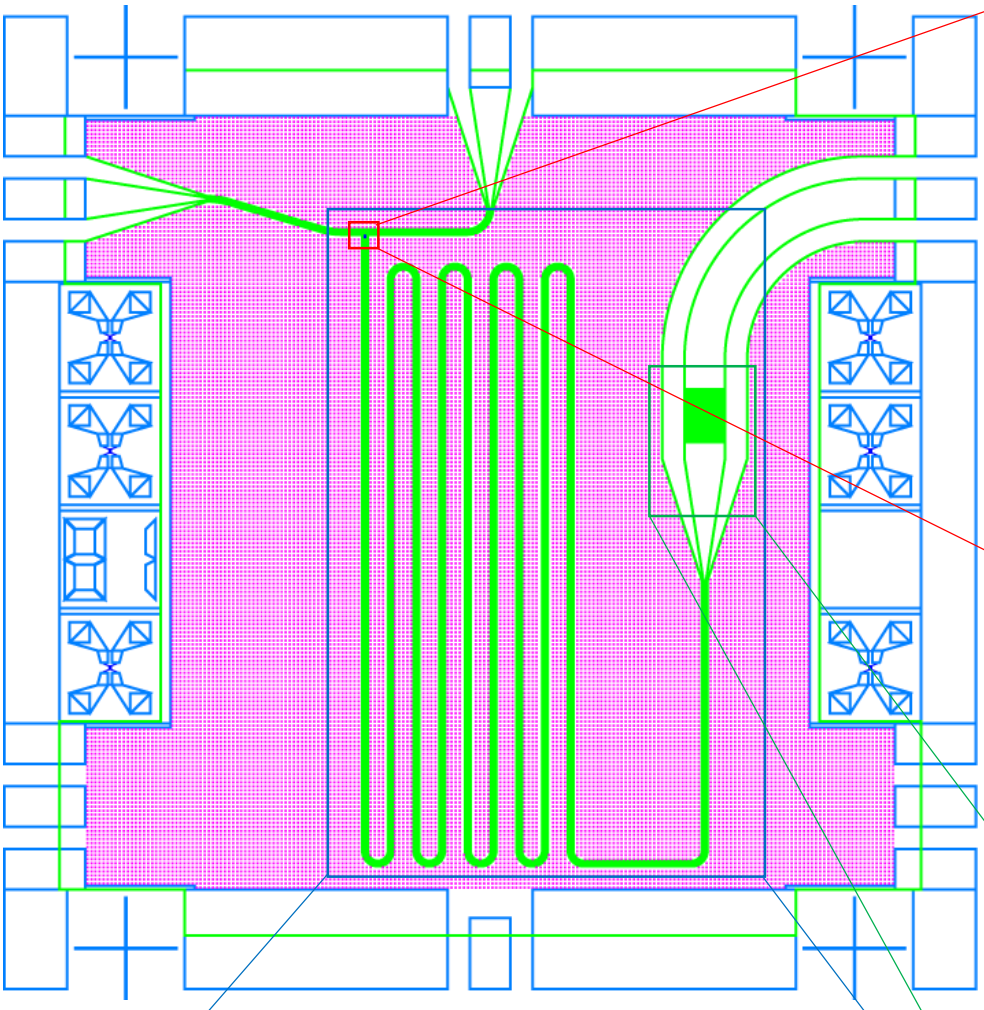

Figure 10. CAD drawing of a JPA sample. A sample designed by Michaël Simoen. The green is the Aluminum pattern including the CPW and SQUID..

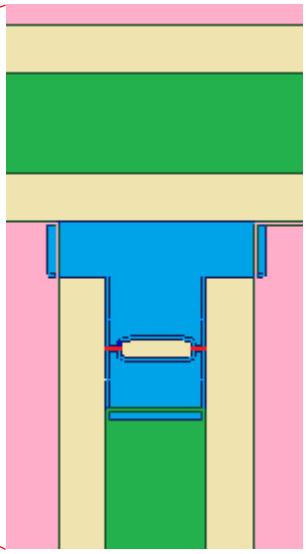

Figure 9, Termination of the resonator. The pink is the ground, the top green strip is the center line of the pump line, and the bottom green strip is the resonator center line. The blue section is the SQUID, with the red strips being the junctions.

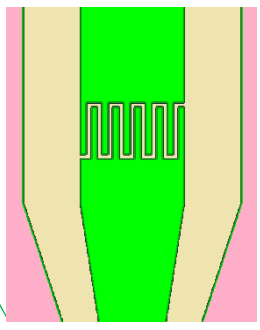

Figure 8, Interdigitated capacitor with 10 fingers, giving a capacitance of 51fF.

The 3cm long meander forms the basis of the resonator. The resonator becomes tunable by having a SQUID as the termination to the ground plane. Next to the SQUID is the pump line where we pass AC current through to pump the resonator for amplification of signal in the resonator.

Design characteristics of the sample:

Resonator Length	R_n of the SQUID	Coupling Capacitance
3 cm	516 Ohm	51 fF

3.1.1. Bare Resonator

In this sample, the quarter-wavelength resonator has a total length of 3cm. We can convert the resonator length to the bare resonator fundamental mode frequency as $f_0 = c/\left(4l\sqrt{\epsilon_{eff}}\right) \approx 1\ GHz$, with an estimated value of $\epsilon_{eff} = 6.8$ S/m. In order for the resonator to fit on a 5x5 mm^2 chip, the resonator is meandered.

3.1.2. Capacitor

The coupling capacitance was implemented as an interdigitated capacitor, as shown in Figure 8, with two separated sets of finger-like conductors interlacing with each other. The capacitance is dominated by the fringing fields due to the thin film geometry, so the usual parallel plate capacitor formula cannot be applied. Approximation formulas can be derived using conformal mapping. However, microwave simulations have to be done in order to accurately design the correct dimension.

The capacitor we used had 10 fingers with 5 on each side. The separation between the fingers was 10μm, the width of fingers was 11μm, and the length of fingers was 100 μm. From microwave simulations, the coupling capacitance was estimated to be 51 fF. Then we can approximate, using the perturbative method in 2.2.3, the Q-factor for the fundamental mode to be around 3000. Then it follows that the 2nd and 3rd harmonics Q-factors would be around 600 and 400 respectively. These are all much lower than the internal Q-factor of the resonator, implying that the resonator should be over-coupled.

3.1.3. SQUID

The unbiased SQUID inductance can be calculated based on the measured R_n. With $R_n = 516\ Ohm$ and assuming 0.25 meV [18] as the superconducting gap for thin-film Aluminum, the inductance is approximately 432 pH. The bare resonator inductance is approximately 12 nH, so the SQUID inductance is a few percent of the resonator's.

3.1.4. Resonance Frequency Change Due to Coupling Capacitance and SQUID

Adding a SQUID between the resonator and the ground, we effectively introduce additional inductance in series with the bare resonator inductance. Similarly, the presence of the coupling capacitor also has the effect of reducing the resonance frequency. The fundamental mode of the resulted resonator therefore will be below the bare resonator frequency 1 GHz. The same will apply to all the higher harmonics of the resonator. A quantitative estimate of resonance frequency reduction can be obtained if the per unit length inductance and capacitance of the bare resonator is known. Here we may assume the fundamental frequency reduction being less than 10% from 1 GHz.

To study multiple modes, we can work with the 2nd and 3rd harmonics whose unbiased resonance should settle within 4 GHz to 8 GHz range. ($f_{m=2} = [2(2) + 1] * 900\ MHz = 4.5\ GHz\ and\ f_{m=3} = [2(3) + 1] * 900\ MHz = 6.3\ GHz$). From section 2.3.2, we can see that as the SQUID is biased and its inductance going up, the inductance will become so large that the resonance frequency approaches zero theoretically. However, this is true only for the fundamental mode. For higher harmonics, we will effectively be tuning the resonator from a quarter-wavelength resonator to approximately a half-wavelength resonator. This implies that the maximum tunable range of the higher harmonics will not exceed 1 GHz below the unbiased frequency. For the 2nd harmonic, we can find the unbiased 2nd harmonic as $f_{m=2} = 4.5\ GHz$. Then the lowest tunable frequency would be above 3.5 GHz.

3.2. Dilution Refrigerator and Microwave Network

3.2.1. Microwave Transmission through the Dilution Refrigerator

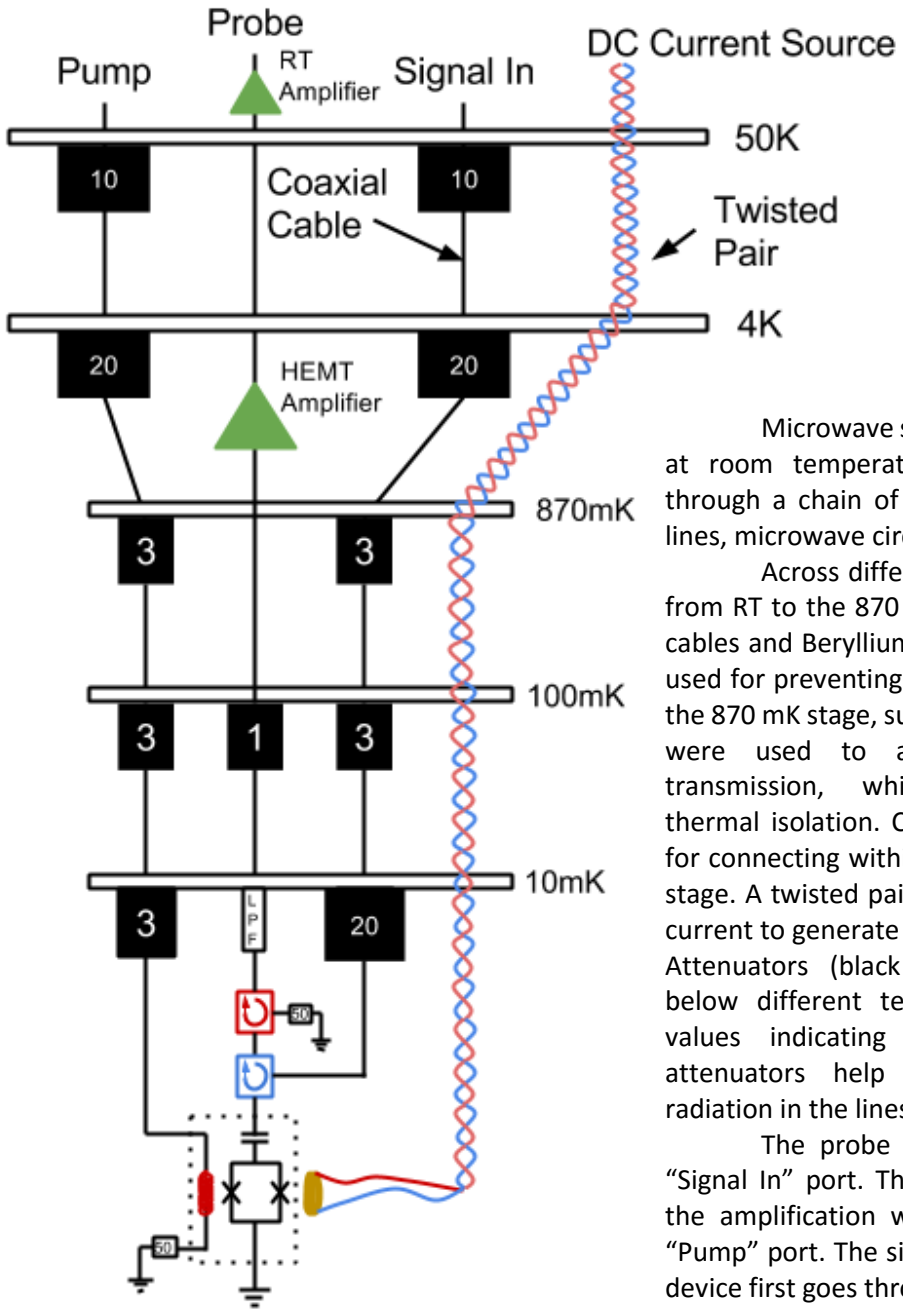

Figure 11. The dilution refrigerator and the microwave network.

Microwave sources and detectors are at room temperature. The signal travels through a chain of microwave transmission lines, microwave circulators and amplifiers.

Across different temperature stages, from RT to the 870 mK stage, stainless steel cables and Beryllium-Copper alloy cables are used for preventing a large heat flow. Below the 870 mK stage, superconducting Nb cables were used to allow low loss signal transmission, while maintaining good thermal isolation. Copper cables were used for connecting within the same temperature stage. A twisted pair was installed to run DC current to generate DC flux in the tuning coil. Attenuators (black boxes) were installed below different temperature stages, with values indicating the attenuation. The attenuators help to cool the thermal radiation in the lines.

The probe signal is injected in the "Signal In" port. The pump signal powering the amplification was sent in through the "Pump" port. The signal going back from the device first goes through the HEMT amplifier, then a room temperature amplifier to the "Probe" port.

3.2.2. Detailed Signal Routing

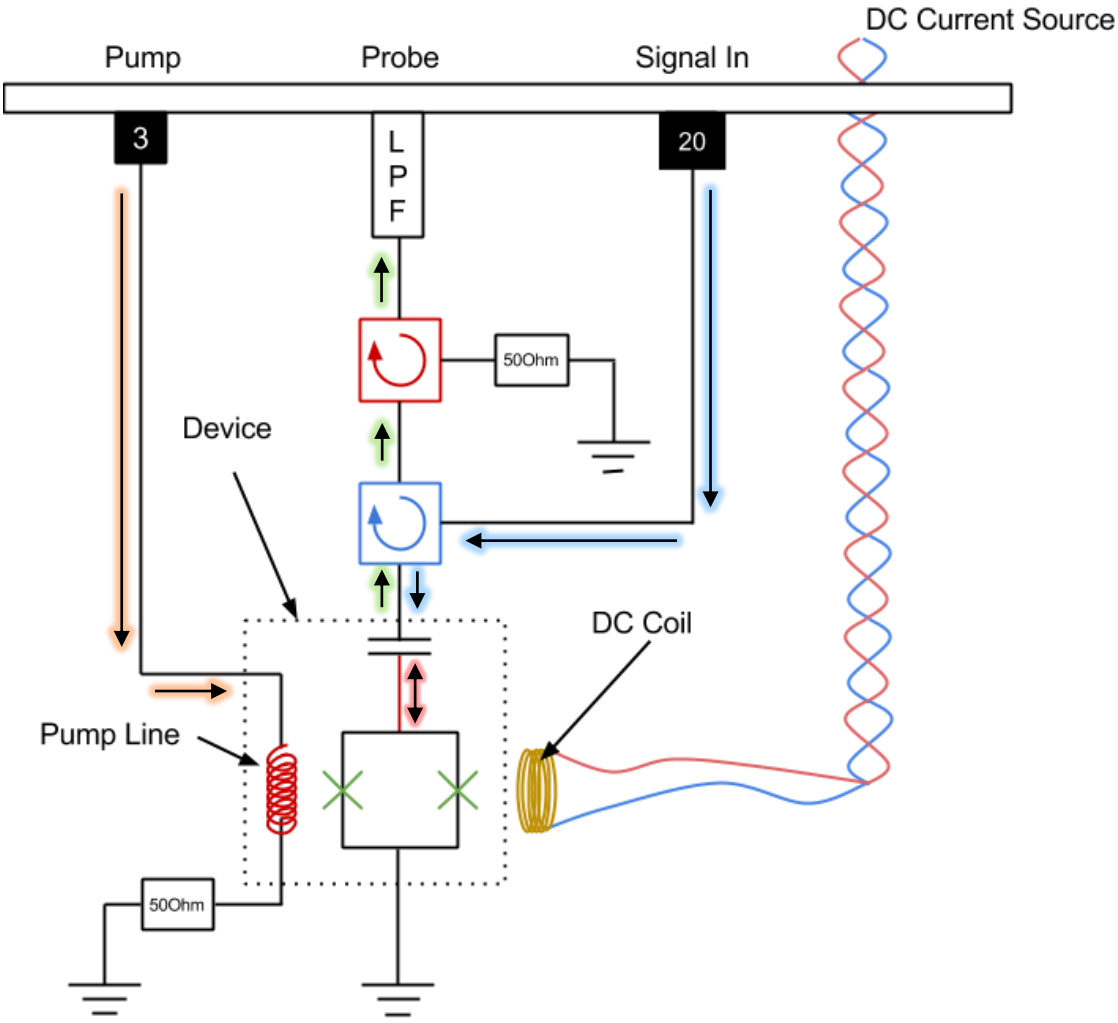

Figure 12. Enlarged image of the bottom temperature stage in the dilution refrigerator. Blue arrows: Input signal to the device; Orange arrows: Pump signal to the device; Red up-down arrow: Resonating signal in the device; Green arrows: Output signal from the device

The probe signal enters through the "Signal In" line and reaches the lower circulator. The circulator directs the signal to the next port, following the arrow direction. The signal thus come out from the bottom port of the lower circulator. The signal is then incident on the device, which is enclosed by dotted line. The signal reflected off of the devices passes through both circulators and the low pass filter on the way to the HEMT amplifier. The circulator prevents the ~4K noise of the HEMT from reaching the device. Pumping of the circuit was achieved by passing a microwave signal running though a transmission line nearby the SQUID on the same circuit.

3.3. Measurement

The parametric amplifier was measured first using vector network analyser (VNA) to characterize its basic parameters. The detailed amplifier performance was then characterized using a dedicated signal generator and vector RF digitizer.

VNA measures the S-parameters between its port 1 and port 2. In a typical measurement, the change in magnitude and phase of the transmitted/reflected signal is measured over a range of frequency. Analyzing the signal reflected from the resonator allows the measurement of the resonance frequency.

As a note, signal power levels at the parametric amplifier sample given here were approximate power levels based on the measured loss of the transmission line. Precise power was difficult to calibrate, so the given levels should be taken as a reference only. When we analysed the gain and signal-to-noise ratio, the relative change in the power level is the most important.

3.3.1. Resonance Frequency Tuning

In this section, we characterize the tunability of the resonator by considering the 2nd and 3rd harmonics, respectively having an unbiased frequency at 4.54 GHz and 6.35 GHz. The signal power at the sample for these measurements was approximately -147 dBm. Flux biasing was done by passing DC current through the coil attached to the sample holder, generating a magnetic flux with an order of magnitude of Φ_0. The VNA was then used to measure the reflection coefficient of the resonator. Moving through resonace the phase of the reflected signal changes by 2π in a frequency range $\sim\omega_2/Q$. This appears as a sharp change in the color scale of Figure 13, indicating the location of the resonace. The below is the tuning curve of the 2nd harmonic.

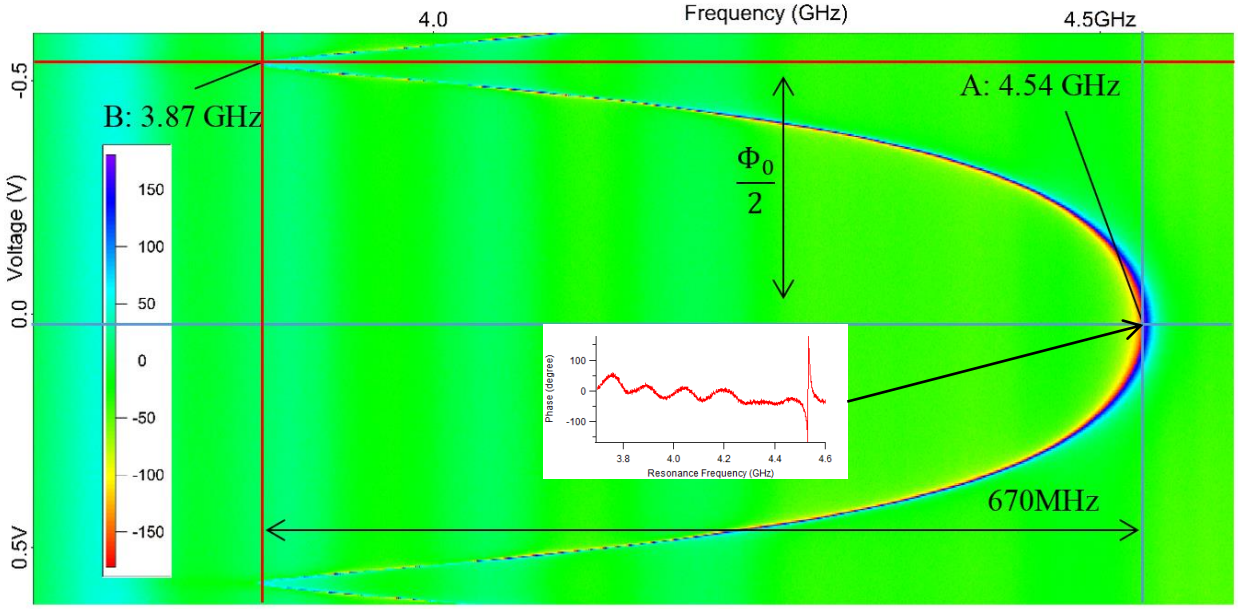

Figure 13. Tuning curve of the 2nd harmonic of the resonator. Different color on the plot indicates the reflected phase at that frequency and flux bias. The resonance frequency is indicated by a sharp color change in the plot, which corresponds to a sharp phase change of 2π. Point A refers to the highest resonance frequency in the tunable frequency range, where the net biasing flux is zero. Point B refers to the lowest resonance frequency of the tuning where the net biasing flux is $\Phi_0/2$.

The DC current was created by connecting a DC voltage source to the superconducting coil (2 Ohm) in series with an 10k Ohm resistor. By the design of the coil, the magnetic field swept was roughly one Φ_0. The power entering the resonator was around $-147dBm$, and was kept constant throughout the whole scan.

The 2nd harmonic can be tuned from $4.54GHz$ to $3.87GHz$, spanning a tunable range of $670MHz$. The tuning of the resonance frequency is symmetric around the peak frequency, where there is no net flux threading the SQUID. From the above plot, the unbiased frequency was slight off the zero bias voltage. This implies that the environmental magnetic field was nonzero around the sample. This is because of the high sensitivity of the SQUID, any stray magnetic field, including the Earth's field, may already be strong enough to have a modulation on the SQUID inductance. Other common sources include ferromagnetic materials in the laboratory, like iron and steel from the furniture and the building.

The tuning curve resembles an $1/|1/cos(x)|$ relationship, as indicated in section 2.3.2. The highest frequency occurs at the net flux being $n\Phi_0$, and the lowest at $(n+1/2)\Phi_0$, and period of the tuning was exactly one Φ_0.

The same principle applies to higher order modes, for instance the 3rd harmonic of the resonator.

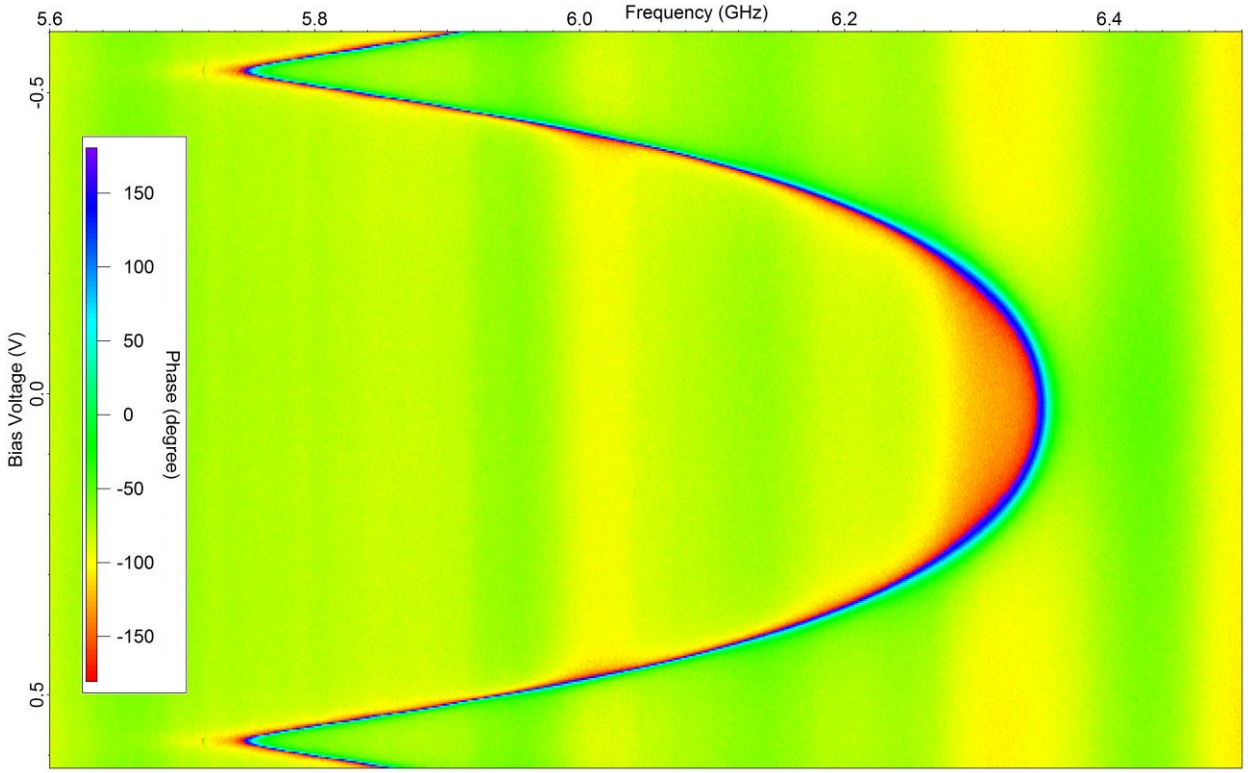

Figure 14. Tuning curve for the 3rd harmonic. Signal was probed from $5.6GHz$ to $6.5GHz$, with the same scan parameter as Figure 13. Resonance frequency were observed at the point as points with a sharp color change in the plot, which corresponded to a sharp phase change due to over-coupling.

The 3rd harmonic was measured in the same magnetic field sweep as the 2nd harmonic. The tunable range of the 3rd harmonic was from $5.75GHz$ to $6.35GHz$.

The resonator can therefore support a wide range of resonance frequencies, and we have control over which frequency to work with. By doing first a flux scan for one Φ_0 like the above, we can obtain a flux tuning curve which tells us the correspondence between the resonance frequency and the bias. With the curve, then we can select a certain frequency by setting the bias. If the magnetic shielding is correctly done, the tuning curve should stay the same throughout the whole cooldown.

From section 2.3.3, the drive strength is depending on the derivative of resonance frequency with respect to flux. In order to obtain enough drive strength for amplification, we often needed to work with a resonance frequency closer to the lowest frequency in the range. Typically, we could get gain by driving the flux from being $0.35\Phi_0$ to $0.45\Phi_0$.

3.3.2. Shift of Resonance Frequency

Once we have chosen a certain resonance frequency, then through the pump line we can inject a microwave signal which creates an oscillating magnetic field near the SQUID. When this pump frequency is exactly double the resonance frequency, we should then obtain parametric amplification. However, we observed that once we started to pump the resonator, there was always a shift in resonance frequency away from the static value. We tried to account for it in two ways.

1. Frequency shift due to magnetic field oscillation

First, by pumping the resonator, we are imposing a frequency oscillation around the static resonance frequency determined by the DC flux bias. As the tuning curve is nonlinear in nature, due to the cos term, the frequency excursion imposed by the pump is not symmetric around the bias point. As indicated by the tuning curves, the frequency should move more towards the lower frequency side, so on average we should see a drop in the resonance frequency. This is, in fact, what was observed. The frequency shift was usually tens of MHz, depending on the mode we were working with, the bias point we took and the pump power we applied.

In Figure 15, we show the pump-induced frequency shift. We pumped the resonator at exactly double the static resonance frequency. The shift at different DC flux biases was studied. We measured the 2nd harmonic with flux bias of $0.1\Phi_0$ and $0.3\Phi_0$.

With $0.1\Phi_0$, we had a resonance frequency of 4.5235 GHz which was close to the highest frequency. The signal power at the cavity was around $-147.5dBm$. We probed the signal frequency over a range large enough to capture the maximum induced shift, in this case it was from 4.46 GHz to 4.54 GHz. The pump frequency was kept unchanged throughout the scan at $2f_{res} = 9.047$ GHz. We then scanned the

pump power from approximately -57 dBm to -37 dBm at the sample to study the shift with different pump power.

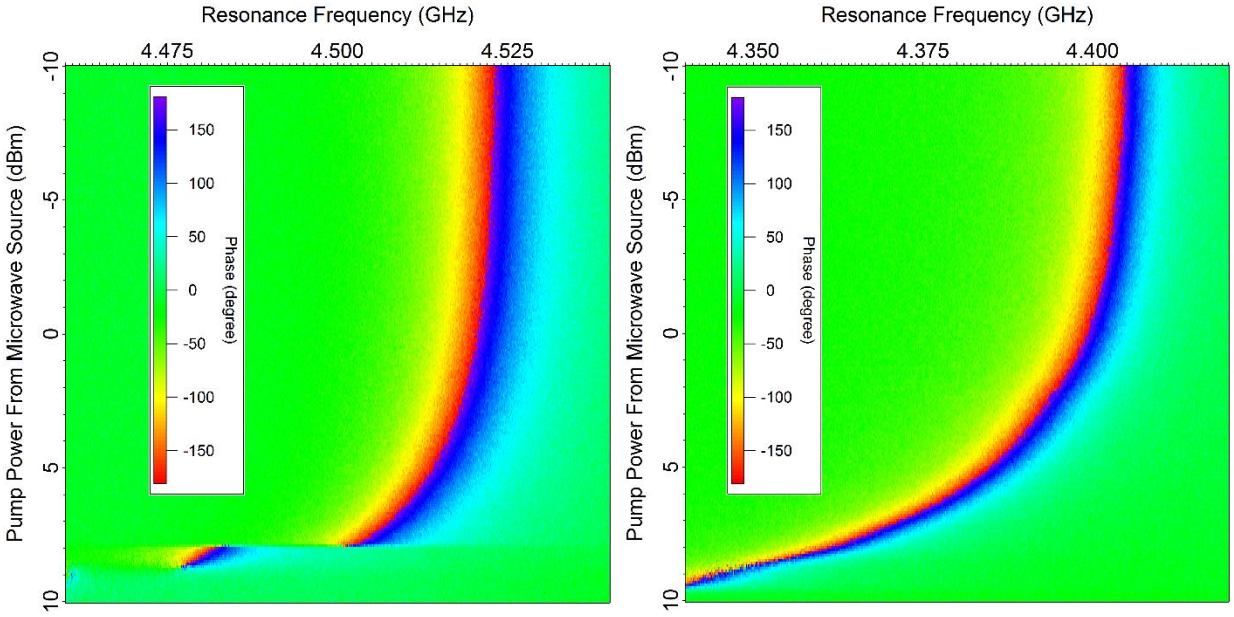

Figure 15, Resonance frequency shift due to flux pumping. Pump power was scanned from -57 dBm to -37 dBm at sample (-10 dBm to 10 dBm from the microwave source), with fixed pump frequency at double of the static resonance frequency. DC flux biases were $0.1\Phi_0$(left) and $0.3\Phi_0$(right). The cut on the $0.1\Phi_0$ may result from a bifurcation of the resonator response.

The frequency shift for a DC flux bias of $0.1\Phi_0$ is tabulated for 4 pump powers($f_{static} = 4.5235GHz$):

Pump power (***dBm***)	$\mathbf{-57}$	$\mathbf{-52}$	$\mathbf{-47}$	$\mathbf{-42}$
Resonance frequency (***GHz***)	4.5228	4.5224	4.5205	4.5140
Shift in frequency (***MHz***)	0.7	1.1	3	9.5

As we expected, the shift is increasing with pump power.

We can compare the above to another scan using a DC flux bias of $0.3\Phi_0$ ($f_{static} = 4.4055GHz$):

Pump power (***dBm***)	$\mathbf{-57}$	$\mathbf{-52}$	$\mathbf{-47}$	$\mathbf{-42}$
Resonance frequency (***GHz***)	4.4048	4.4033	4.399	4.3844
Shift in frequency (***MHz***)	0.7	2	6.5	21

On comparing, we found that the shift was more pronounced with a larger DC flux bias, which corresponded to a lower static resonance frequency. Therefore in order to get gain, we would need to adjust the pump frequency to bring the pump into resonance with the shifted frequency accordingly to the bias points.

2. Frequency shift due to increasing signal power

Another reason for the frequency shift is related to the signal power in the resonator. In section 2.1.3 we were treating the SQUID inductance with the lowest order approximation. For a larger signal power, next order nonlinear terms will start to have significant contribution. The resonator can then be modelled by the well-known Duffing oscillator. The resonator acts like a “softening spring” and resonance shifts to lower frequency with increasing signal power inside.

To study the effect of signal power on resonance frequency shift, we scanned the signal power with no pump signal applied. This was done at zero DC flux bias and $0.33\Phi_0$. We set the DC flux to approximately zero, giving a resonance frequency of 4.533 GHz. We stepped the signal power in 1 dBm increments, increasing from -157 dBm to -97 dBm at the sample (-60dBm to 0dBm from the VNA).

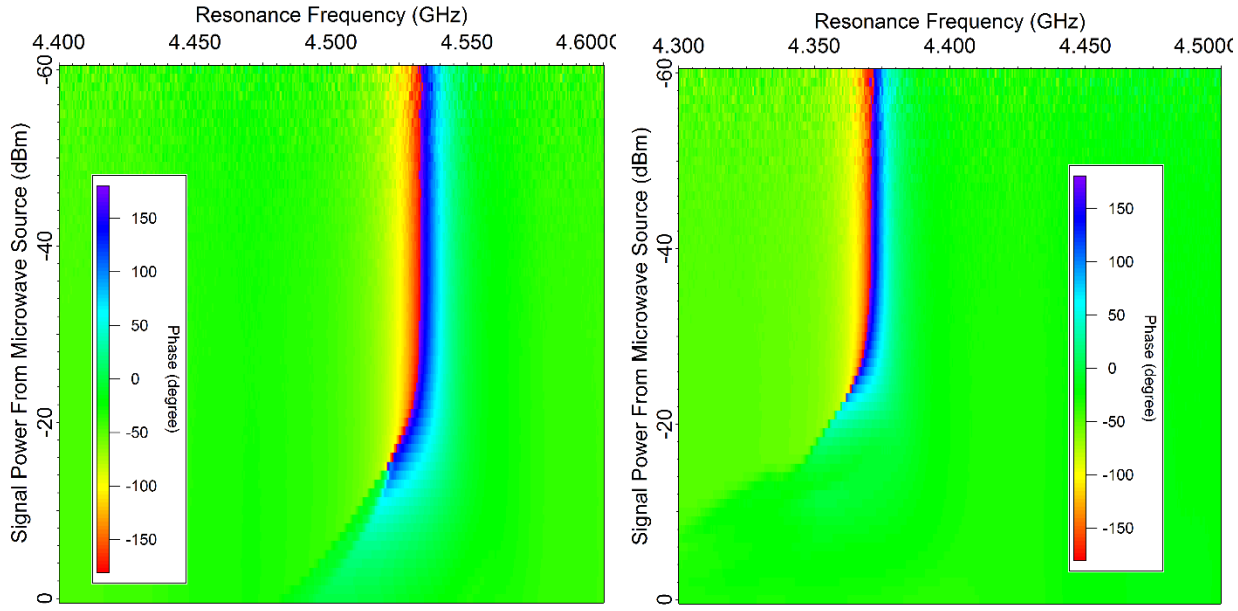

Figure 16. Scan of signal power. At zero flux bias(left) and $0.33\Phi_0$(right), from -157 dBm to -97 dBm at the sample (-60 dBm to 0 dBm from the microwave source).

The results are tabulated below for the two bias points.

For zero flux bias($f_{static} = 4.533GHz$):

Signal power (***dBm***)	**−132**	**−127**	**−122**	**−117**
Resonance frequency (***GHz***)	4.5330	4.5330	4.5320	4.5290
Shift in frequency (***MHz***)	0	0	1	4

Biased at $0.33\Phi_0$ ($f_{static} = 4.371GHz$):

Signal power (***dBm***)	**−132**	**−127**	**−122**	**−117**
Resonance frequency (***GHz***)	4.3705	4.3695	4.3650	4.3560
Shift in frequency (***MHz***)	0.5	1.5	6	15

The shift in resonance frequency showed a dependence on the DC flux bias chosen. With zero bias, the resonance frequency started to shift at a signal power of -129 dBm. At $0.33\Phi_0$, the shift started from a lower signal power of -134 dBm. With another 13 dB increase in signal power, the amount of frequency shift on the two bias points were 5.5 MHz and 9.5 MHz respectively for zero bias and $0.33\Phi_0$. The second bias had a larger shift as expected, as the critical current was smaller and nonlinear terms become important more quickly.

We can also see from the color plot, the sharp color change disappeared when the signal power was further increased. It was -112 dBm for zero bias, and at -120 dBm for $0.33\Phi_0$. As the color denoted phase change, this was an indication that the resonator was no longer being over-coupled, caused by an increased internal

loss inside the cavity. As the signal power went up, it approached the critical current of the Josephson junctions, which introduced loss. This implies that there is an upper limit on the signal power we can use.

Because of the combined effects of these frequency shifts, we cannot get gain from the device simply by selecting a certain DC bias and pump at double the resonance frequency. Accordingly, we had to perform a parametric scan to see at what combinations of pump frequency, pump power and DC flux bias we achieved signal gain.

3.3.3. Scanning for Amplification

There are basically 4 parameters to scan: DC flux bias, signal power, pump power and pump frequency. It would take a very long time to scan all four. With the understanding of the previous sections, we can however limit the region of the scan.

To simplify the scan, we probed over a frequency range from 3.7 GHz to 4.6 GHz, and fixed a low signal power (-147 dBm) which did not induce a frequency shift. We also stuck to a specific bias of $0.389\Phi_0$, where the static resonance frequency was 4.2488 GHz. We then swept the pump frequency from 8.4 GHz to 8.6 GHz, and the pump power from -47 dBm to -34 dBm at the sample. At the VNA, we measured the reflected signal power and compared its magnitude against the signal looking for gain.

Amplification started to appear with a pump power above -42 dBm and a pump frequency below 8.46 GHz. This profile was consistent with the previous findings, that the pumping and a stronger signal would give rise to a decrease in resonance frequency. Knowing the parameters that gave amplification, we focused on this range and performed a more detailed scan, measuring the gain and signal-to-noise ratio. We further studied the threshold between parametric amplification and parametric oscillation.

3.3.4. Amplification Analysis

In the following measurement we switched from the VNA to a continuous wave generator and a vector RF digitizer, which provided the data needed to characterize the signal-to-noise ratio. We probed with a continuous wave tone and then amplified the reflected signal and digitized it over a narrow frequency range centered at the probe frequency we sent, with a resolution bandwidth of 500 Hz. The power we sent to the resonator was around -147 dBm. From the measured power spectrum, we could extract the gain at the probe frequency and the change in signal-to-noise ratio.

Based on the previous gain region we found, we scanned the pump frequency from 8.39 GHz to 8.46 GHz, stepped the pump power from -45 dBm to -34 dBm at the sample. We probed at a signal frequency detuned 50 kHz away from half of the pump frequency($i.e.\ f_{probe} = f_{pump}/2\ + 50kHz$). With this detuning, we expect nondegenerate amplification that is phase independent. We plotted the peak magnitude of the detected signal power over the range of the pump power and frequency we probed. Note that at high powers we expect a transition to parametric oscillation. This transition can be identified from the shape of the power spectrum.

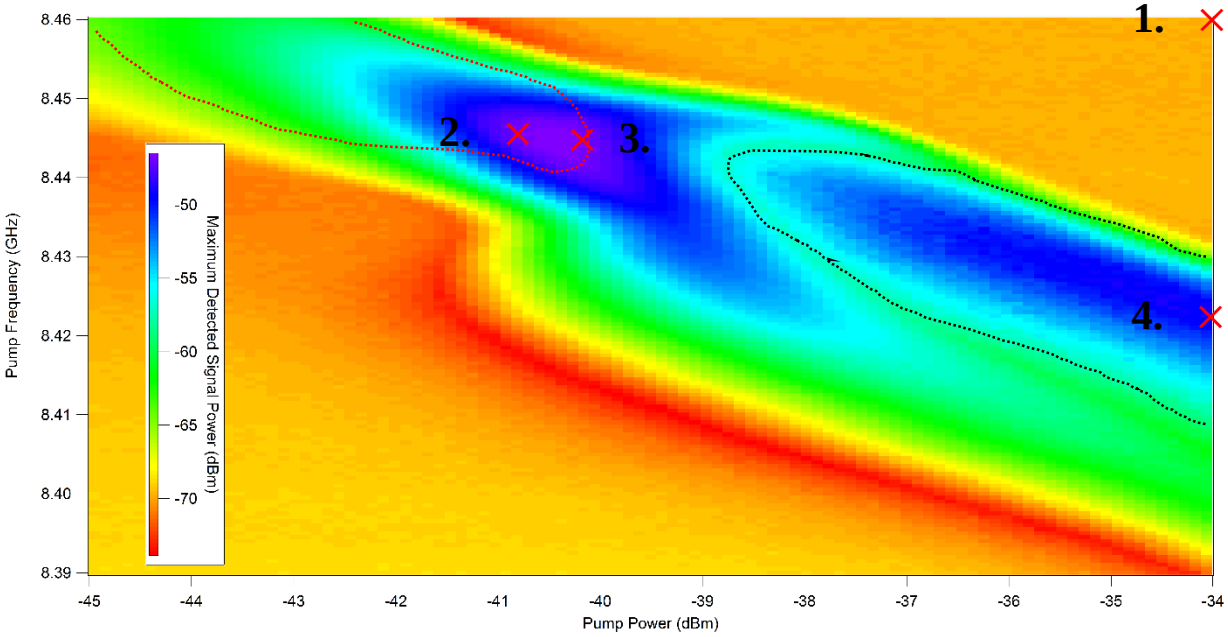

Figure 17. Plot of maximum detected signal power against the scanned pump power and frequency. Pump power was stepped from $-45dBm$ to $-34dBm$ at the sample, and pump frequency swept from $8.39GHz$ to $8.46GHz$. The region with the signal-to-noise ratio improvement more than 5dB is enclosed by the red dotted line on left side. The dark dotted line on the right encloses the region where the parametric oscillation are clearly dominating.

We will focus on the 4 points noted with a $cross$ on the parametric plot for the following analysis, with the corresponding coordinate (pump power, pump frequency) and result [gain, signal-to-noise ratio]:

1. No amplification nor oscillation (reference point) (-34.0 dBm, 8.460 GHz) [0.00 dB, 14.8 dB]
2. Maximum signal-to-noise ratio improvement (-40.8 dBm, 8.445 GHz) [17.0 dB, 24.3 dB]
3. Maximum amplification (-39.8 dBm, 8.444 GHz) [23.0 dB, 22.6 dB]
4. Spontaneous parametric oscillation (-34.0 dBm, 8.423 GHz) [1.90 dB, N/A]

1. No amplification nor parametric oscillation (-34.0 dBm, 8.460 GHz) [0.00 dB, 14.8 dB]

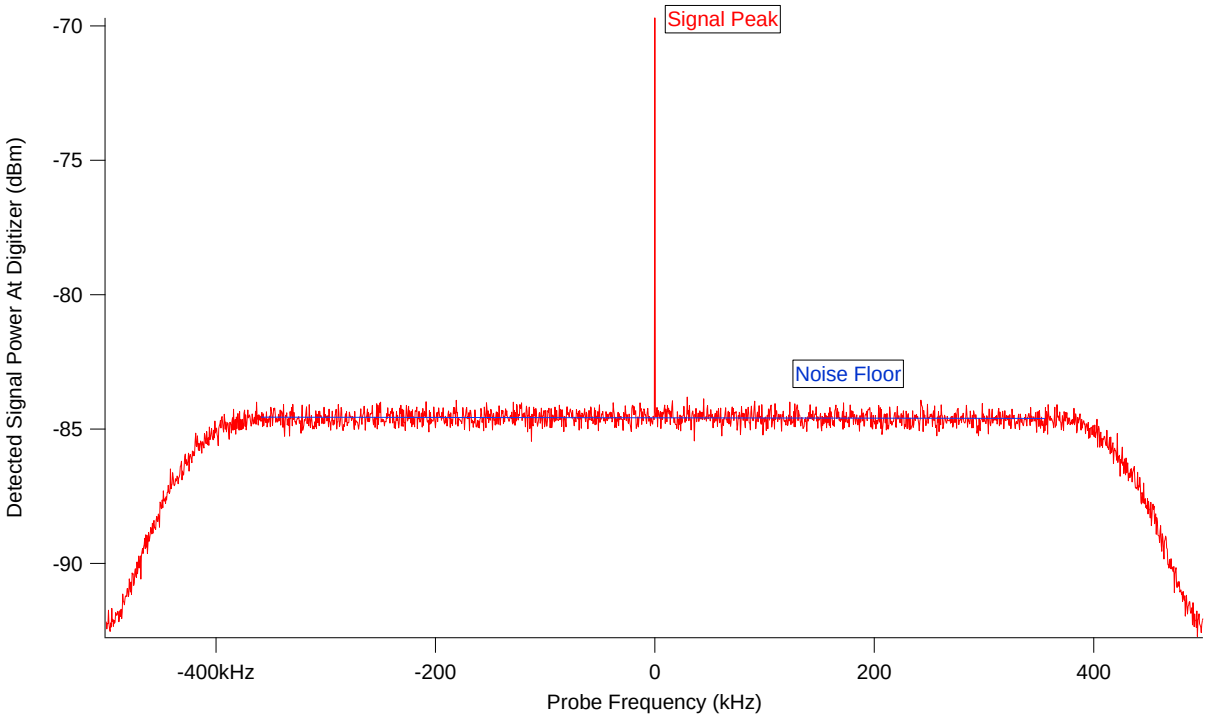

This plot displays the power spectrum measured at the position of *cross* 1 in Figure 17. The power spectrum is centered at the probe signal frequency. At this coordinate, the pump parameters are far from the active region, and we can characterize the baseline transmission and noise floor of the system. We found the signal power to be -69.7 dBm compared to a noise floor of -84.5 dBm. This gives a baseline signal-to-noise ratio of 14.8 dB determined by the noise of the HEMT amplifier.

This reference point could then be used for comparing to other configurations, in order to characterise the gain and signal-to-noise ratio improvement given by the parametric amplifier.

2. Maximum signal-to-noise ratio improvement (-40.8 dBm, 8.445 GHz) [17.0 dB, 24.3 dB]

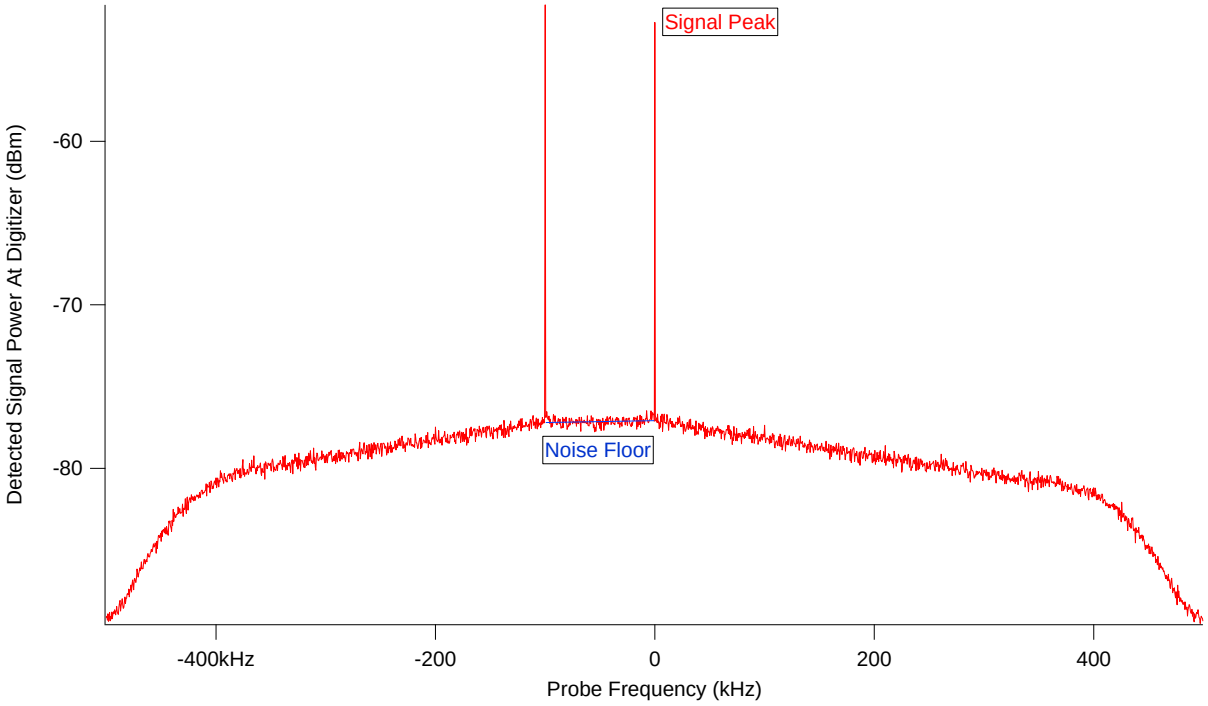

With this configuration, we saw nondegenerate amplification. Energy conservation requires the creation of an idler frequency component (left) which is symmetric with the signal frequency around half the pump frequency. The signal and idler frequencies sum to the pump frequency. As the signal was set to a detuning of +50 kHz, we expected the signal and idler to be 100 kHz apart, which was the observed.

The signal power after amplification was $-52.7dBm$, which implied a gain of $17dB$. The new signal-to-noise ratio was found to be 24.3 dB, which was an improvement of 9.5 dB.

3. Maximum amplification (-39.8 dBm, 8.444 GHz) [23.0 dB, 23.6 dB]

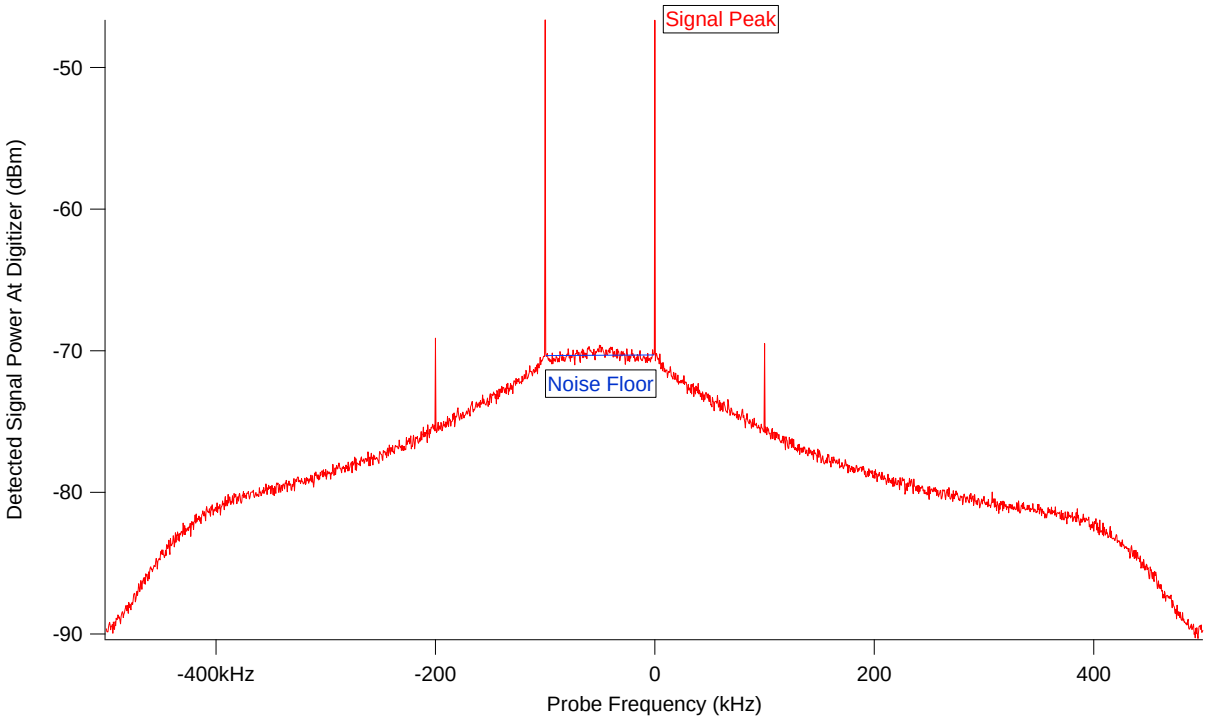

At this working point, we saw the maximum gain of 23 dB. However, the signal-to-noise ratio improvement dropped to 8.8 dB, lower than the previous configuration.

The gain is enough for the parametric amplifier noise to dominate. Signal may be compressed relative to noise due to a maximum allowed signal power in the resonator as observed in section 3.3.2. As the signal and idler were getting stronger, they would have a modulation effect on the resonance. This could give rise to frequency mixing and created the two side band frequencies we observed. The signal to noise ratio improvement would have been even smaller if the side band peaks were considered the peak noise level.

4. Spontaneous parametric oscullation (-34 dBm, 8.423 GHz) [1.9 dB, N/A]

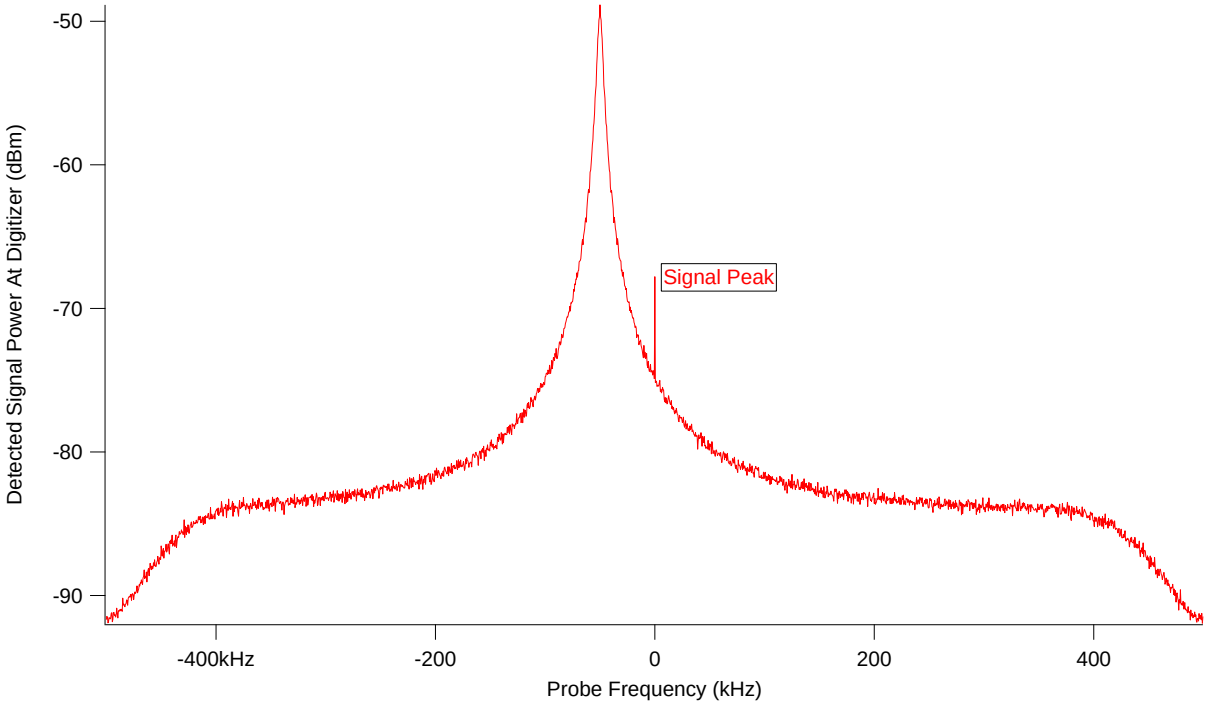

By pumping even harder, the deformation of the noise floor becomes more obvious and the peak becomes higher. When the peak of the noise floor is higher than the signal peak, the resonator is clearly oscillating and the gain at the signal frequency is minimized. At this point the device no longer acts as an amplifier.

This implies that the pump power for parametric amplification has an upper bound. A stronger pump signal does not necessarily provide a large amplification nor signal to noise ratio improvement. As seen in the parametric scan in Figure 17, going beyond a certain pump power around -39 dBm led to spontaneous parametric oscillation, which was indicated roughly by the boundary between the left and right blue sections in the color plot.

4. Conclusion

In this work, we have measured a flux-pumped variant of a JPA implemented with a quarter-wavelength tunable resonator. We characterized the frequency tunability of the resonance of two harmonics. We then focused on the 2nd, studying the induced resonance frequency shift due to flux pumping and strong signal power. We further characterized the device as a parametric amplifier, mapping out various working points, measuring the gain and signal-to-noise.

We found the JPA to have a signal-to-noise ratio performance significantly higher than the well-developed, commercially available HEMT amplifiers. This suggests its potential to be developed as the new standard for low-noise amplification for microwave signal in cryogenic environment. This is especially suitable for the rapid development of superconducting quantum computation and quantum networks.

We conclude that the biasing of the flux-pumped JPA requires precise control. The JPA is highly sensitive to parameters, including the pump and signal power, the DC flux bias and pump frequency. They combine to give a narrow region in the parameter space where the device can be operated as a parametric amplifier. Failure in understanding the device will result in poorly optimized gain or spontaneous parametric oscillations.

In view of the above, we expect to follow up by quantifying the noise performance of the JPA. This can be done by using a shot noise tunnelling junction, from which we can determine exactly the system's noise temperature and thus compare the JPA's added noise to the standard quantum limit. We believe this will allow a better understanding of the device.

Bibliography

[1] T. P. Orlando, J. E. Mooij, Lin Tian, Caspar H. van der Wal, L. S. Levitov, Seth Lloyd, and J. J. Mazo, "Superconducting persistent-current qubit," *Physical Review B,* no. 60, 1999.

[2] I. Chiorescu, Y. Nakamura, C. J. P. M. Harmans, J. E. Mooij, "Coherent Quantum Dynamics of a Superconducting Flux Qubit," *Science,* vol. 299, pp. 1869-1871, 2003.

[3] A. Wallraff, D. I. Schuster, A. Blais, L. Frunzio, R.- S. Huang, J. Majer, S. Kumar, S. M. Girvin & R. J. Schoelkopf, "Strong coupling of a single photon to a superconducting qubit using circuit quantum electrodynamics," *Nature,* vol. 431, pp. 162-167, 2004.

[4] R. J. Schoelkopf, S. M. Girvin, "Wiring up quantum systems," *Nature,* vol. 451, pp. 664-669, 2008.

[5] Hanhee Paik, D. I. Schuster, Lev S. Bishop, G. Kirchmair, G. Catelani, A. P. Sears, B. R. Johnson, M. J. Reagor, L. Frunzio, L. I. Glazman, S. M. Girvin, M. H. Devoret, and R. J. Schoelkopf, "Observation of High Coherence in Josephson Junction Qubits Measured in a Three-Dimensional Circuit QED Architecture," *PHYSICAL REVIEW LETTERS,* vol. 107, 2011.

[6] A. A. Clerk, M. H. Devoret, S. M. Girvin, F. Marquardt, and R. J. Schoelkopf, "Introduction to quantum noise, measurement, and amplification," *REVIEWS OF MODERN PHYSICS,* vol. 82, no. 2, 2010.

[7] C. M. Wilson, T. Duty, P. Delsing, "Parametric oscillators based on superconducting circuits," in *Fluctuating Nonlinear Oscillators: From Nanomechanics to Quantum Superconducting Circuits,* 2012.

[8] Hatridge, M. and Vijay, R. and Slichter, D. H. and Clarke, John and Siddiqi, I.;, "Dispersive magnetometry with a quantum limited SQUID parametric amplifier," *Phys. Rev. B,* vol. 83, no. 13, p. 134501, 2011.

[9] Krantz, Philip, "Parametrically pumped superconducting circuits," 2013.

[10] J. Bardeen, L. N. Cooper, and J. R. Schrieffer, "Theory of Superconductivity," *Phy. Rev.,* vol. 108, no. 5, 1957.

[11] Josephson, B. D., "The discovery of tunnelling supercurrents," *Reviews of Modern Physics,* vol. 46, no. 2, 1974.

[12] Charles P. Poole Jr., Ruslan Prozorov, Horacio A. Farach, Richard J, Creswick, Superconductivity (3rd edition), Elsevier, 2014.

[13] Pozar, David M., Microwave Engineering, John Wiley & Sons, Inc, 1998.

[14] Fredrik Persson, "Fast dynamics and measurements of single-charge devices," 2013.

[15] Denker, Bernard Yurke and John S., "Quantum network theory," *PHYSICAL REVIEW A,* vol. 29, no. 3, 1984.

[16] M. Sandberg, C. M. Wilson, F. Persson, T. Bauch, G. Johansson, V. Shumeiko, T. Duty, and P. Delsing, "Tuning the field in a microwave resonator faster than the photon lifetime," *Applied Physics Letter,* vol. 92, 2008.

[17] Fox, Mark, Quantum Optics, Oxford, 2006.

[18] N A Court, A J Ferguson1 and R G Clark, "Energy gap measurement of nanostructured aluminium thin films for single Cooper-pair devices," *IOP Science,* no. 21, 2008.